Int. J. Impact Engng Vol. 5, pp. 33–59, 1987
Printed in Great Britain

0734-743X/87 $3.00 + 0.00
Pergamon Journals Ltd.

AN OVERVIEW OF THE THEORY OF HYDROCODES

Charles E. Anderson, Jr.

Southwest Research Institute
San Antonio, TX

ABSTRACT

Hydrocodes are large computer programs that can be used to simulate numerically highly dynamic events, particularly those which include shocks. Lagrangian and Eulerian descriptions are reviewed, and advantages and disadvantages are summarized. The question of how to best represent the continuum equations on a finite computer is answered by summarizing the topics of accuracy and stability. The concept of artificial viscosity is introduced to permit the continuum code to deal with the discontinuities of shocks. Finally, a review of the treatment of materials, i.e., equation of state and constitutive response, including failure, is presented.

INTRODUCTION

Classical continuum mechanics attempts to describe the dynamics of a continuous media with a set of differential equations established through the application of the principles of conservation of mass, momentum, and energy from a macroscopic point of view. An equation of state relates the density (or volume) and internal energy (or temperature) of the material with pressure. A constitutive relation describes the particular nature of the material by relating the stress in the material with the amount of distortion (strain) required to produce this stress. The constitutive relation may include strain rate effects, work hardening, thermal softening, etc.

The differential equations relate material density ρ, velocity v_i, specific total energy e, the stress tensor σ_{ij}, and external body forces per unit mass f_i, where the subscripts represent standard tensorial notation. Two fundamental descriptions of the kinematic deformation of continuous media exist: the Eulerian (spatial) and Lagrangian (material) description. The conservation equations for the two descriptions are:

	Lagrangian	Eulerian	
Conservation of Mass	$\frac{D\rho}{Dt} + \rho \frac{\partial v_i}{\partial x_i} = 0$	$\frac{\partial \rho}{\partial t} + \frac{\partial}{\partial x_i}(\rho v_i) = 0$	(1)
Conservation of Momentum	$\frac{Dv_i}{Dt} = f_i + \frac{1}{\rho}\frac{\partial \sigma_{ji}}{\partial x_j}$	$\frac{\partial v_i}{\partial t} + v_j \frac{\partial v_i}{\partial x_j} = f_i + \frac{1}{\rho}\frac{\partial \sigma_{ji}}{\partial x_j}$	(2)
Conservation of Energy	$\frac{De}{Dt} = f_i v_i + \frac{1}{\rho}\frac{\partial}{\partial x_j}(\sigma_{ij} v_i)$	$\frac{\partial e}{\partial t} + v_i \frac{\partial e}{\partial x_i} = f_i v_i + \frac{1}{\rho}\frac{\partial}{\partial x_j}(\sigma_{ij} v_i)$	(3)

The summation convention is implied by the repeated indices. In Eqs. (1-3), the "ordinary" mechanical effects have been considered, but electromagnetic, chemical, and heat conduction effects have been ignored.

The differences between the two sets of equations are inherent in the definition of the derivative D/Dt:

$$\frac{D}{Dt} = \frac{\partial}{\partial t} + v_i \frac{\partial}{\partial x_i} \tag{4}$$

which goes by the various names of material derivative, substantial derivative, or total time derivative. The significance of this derivative will be discussed in the next section.

The total specific energy is the sum of kinetic energy and specific internal energy E:

$$e = \frac{1}{2} v_i v_i + E \tag{5}$$

Equation (3) is often rewritten in terms of the specific internal energy:

Lagrangian	Eulerian
$\frac{DE}{Dt} = \frac{P}{\rho^2}\frac{D\rho}{Dt} + \frac{1}{\rho} s_{ij} \dot{\varepsilon}_{ij}$	$\frac{\partial E}{\partial t} + v_i \frac{\partial E}{\partial x_i} = \frac{P}{\rho^2}\left(\frac{\partial \rho}{\partial t} + v_i \frac{\partial \rho}{\partial x_i}\right) + \frac{1}{\rho} s_{ij} \dot{\varepsilon}_{ij}$

(6)

where s_{ij} and $\dot{\varepsilon}_{ij}$ are the stress deviators and strain rates, respectively, and P is the hydrostatic pressure.

Two more expressions are required to complete the set of equations, an equation of state, and a constitutive model:

$$P = P(\rho, E) \qquad \sigma_{ij} = f(\varepsilon_{ij}, \dot{\varepsilon}_{ij}, E, K) \tag{7}$$

The equation of state accounts for compressibility effects (changes in density) and irreversible thermodynamic processes such as shock heating. The constitutive model, in general, permits the stress to be a function of strain ε_{ij}, strain rate effects $\dot{\varepsilon}_{ij}$ (both in loading and unloading, i.e., stress relaxation), internal energy E (thermal softening), and damage K. Of course, before a solution can be obtained, appropriate boundary and initial conditions must also be prescribed.

The set of coupled, highly nonlinear equations represented by Eqs. (1-7) has been solved exactly for only a dozen or so problems where certain simplifying restrictions have been invoked (e.g., incompressible flow, inviscid flow, irrotational flow, potential flow). Approximate or asymptotic solutions have been obtained by discarding certain terms, and these solutions have practical utility in certain physical circumstances, for example, boundary layer theory. Perturbation theory and singular perturbation theory have been used to obtain solutions over a restricted range where the assumptions imposed are valid. In general, however, analytical solutions rely on linearity, symmetry, and a small number of variables. But, there exist many problems of practical interest whose solutions are not amenable to these techniques; the full set of coupled equations must be solved simultaneously. With the advent of digital computers, thousands of mathematical operations can be performed quickly; thus, numerical techniques provide a method of obtaining solutions.

Computer programs which handle the propagation of shock waves and compute velocities, strains, stresses, etc., as a function of time and position are called "hydrocodes." Early formulations did not include strength effects. Thus, metals were treated as a fluid, with no viscosity, and the expression, "hydrodynamic computer code" came into being; with time, this was shortened to hydrocodes. Hydrodynamic computer codes can compute the approximate response of a material object providing the pressures are sufficiently high that strength effects can be ignored. However, in developing better predictive capabilities, material modeling has become more sophisticated.

These computer programs can predict the response of a penetrator and target from first principles. They are powerful tools to the analyst; they can provide insight and help explain phenomena observed in experiments. They can be used to test hypotheses concerning fundamental mechanisms, and be used in a systematic application to obtain the influence of variables. They can be used to extend experimental data by performing parametric variation of variables; they can be used as an alternative to experiments; and, they may be the only recourse in the extreme high velocity regimes since current launch techniques do not permit the velocities such as may be encountered outside the earth's atmosphere. In one sense, hydrocodes are the best instrumented experiment. By simulating the experiment numerically, strains, strain rates, velocities, displacements, stresses, etc., as a function of time and space are obtained.

There are several good articles which review and compare one, two, and three dimensional hydrocodes (Mescall, 1974; Belytschko, 1975; Herrmann, 1975; Jonas and Zukas, 1978; Zukas, 1980; Zukas et al., 1981; Zukas, et al., 1982). The reader is referred to these articles for further information. The remainder of this paper is concerned with the numerical issues of hydrocodes.

EULERIAN AND LAGRANGIAN DESCRIPTIONS

The Eulerian description is a spatial description; the Lagrangian description is a material description. From a computational point of view, a few less derivatives need to be computed in

the Lagrangian description, e.g., Eqs. (1-3). Fundamentally, however, there are significant differences between the two mathematical descriptions and their numerical solutions. In the numerical representation of the differential equations, it becomes very easy to visualize the distinction between these two descriptions, and understand inherent advantages and disadvantages of each.

Solution of Eqs. (1-7) first requires that the differential equations be discretized. A lattice of points, or grid, is generated to approximate the geometry of interest. If adjacent points are connected by lines, the area or volume enclosed by connecting adjacent points in the grid is referred to as cells.

To obtain an Eulerian or spatial description, one would measure (or compute), as time progresses, velocity, pressure, density, temperature, etc., at the fixed points of the grid. All grid points, and consequently cell boundaries, remain spatially fixed with time. Mass, momentum, and energy flow across cell boundaries. The quantities of flow into and out of a cell are used to compute the new mass, pressure, velocity, energy, etc., of that cell. In this formulation, the cell volume is obviously an invariant since points remain fixed in space.

In the Lagrangian description, however, the grid points are attached or fixed to the material and move with the local material velocity. Velocity, pressure, density, temperature, etc., are computed as time progresses for each discrete point in the continuum. Adjacent points can be stretched or come closer together, as in a spring, depending upon the forces applied. Mass, momentum, and energy are transported by material flow--the grid points move relative to a fixed spatial coordinate system. In mathematical terminology, the grid points follow particle paths of points in the material. In this formulation, mass within a cell is invariant, but the volume of the cell may change with time because of expansion or compression of the material.

Again note the distinction between the two mathematical descriptions. For example, in computing the density of a cell, $\rho = M/V$, where M is the mass within the cell of volume V, the Eulerian description has a constant volume, V, and the mass changes as more or less mass accumulates in the cell due to mass flow across the boundaries of the cell. The density would decrease if more mass flowed out of a cell during a time step, Δt, then flowed into the cell. In the Lagrangian description, the mass M is a constant, and the volume of the cell changes due to the movement of the boundaries firmly attached to the moving material. For example, the density would increase as the cell is compressed.

In Lagrangian calculation, the mesh is generated to approximate the materials of interest with points (Lagrangian lines) placed along exterior boundaries (free surfaces) and material boundaries. Boundary conditions at free surfaces and contact surfaces between different materials are straightforward. The positions of free surfaces and contact surfaces are automatically determined in the computations, and, thus, are one of the features which makes the Lagrangian formulation so useful. For example, Fig. 1 depicts the normal impact of a steel cylindrical projectile against an aluminum plate using a Lagrangian grid. Obviously, the free surfaces are well-defined, as well as the ability to clearly distinguish steel and aluminum cells. Likewise, if the plate (or projectile) were made of layers of materials, the different material interfaces could be easily distinguished, since each grid cell is uniquely a specific material.

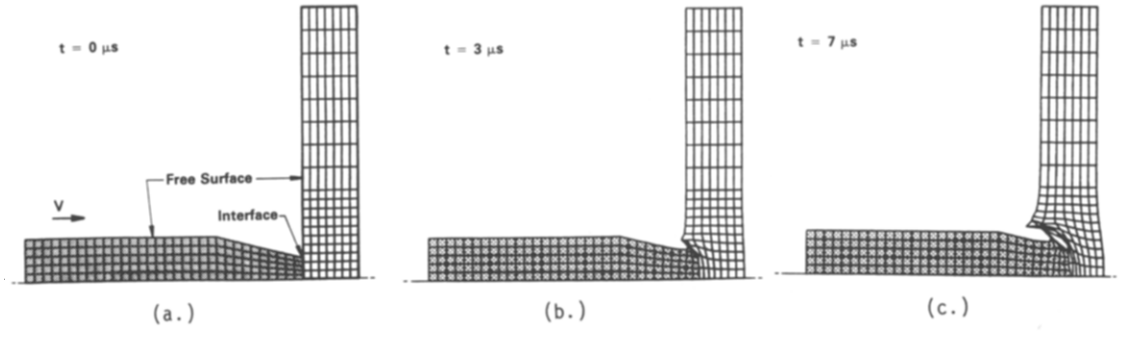

Fig. 1. Lagrangian grid.

Behavior at material interfaces, such as the opening and closing of voids, can be computed by a Lagrangian calculation by providing spatial slidelines. Slidelines are generally used when large transverse motion along a material interface is expected (Wilkins, 1964; Swegle, 1978). Opposite sides of the sliding interface are often referred to as the "master" and "slave" surfaces. The

master-slave pair is called a slideline. The master surface is advanced using its own force field and the force field of the slave surface. The slave surface is then brought back into contact with the master. The normal components of velocity are assumed to be continuous across the slideline, but the tangential components may be discontinuous. Points may be tied initially and allowed to break if some criterion is met. Friction effects can be included for motion along slidelines. Of course, the code user must understand the problem well enough to know where slidelines would naturally occur; otherwise, these effects will not be modeled accurately.

Another important advantage of the Lagrangian description is in its ability to follow the history of a material particle. A material whose properties depend upon its previous history can be modeled. Thus, the Lagrangian description allows an excellent treatment of material models (constitutive relations) and failure models, e.g., strain hardening and total plastic work.

Lagrangian codes can have severe difficulties, however, where large grid distortions occur, such as turbulent flow and high velocity impacts. In the Lagrangian grid, the mesh points follow the motion of particles of mass. For example, in an impact problem, the computational mesh becomes severely distorted near the projectile/target interface, Fig. 1b and 1c. Sometimes a zone may flip back on itself resulting in a computed negative mass. Even with a slideline at the projectile/target interface, the numerical calculations bog down during the first few microseconds. The time step becomes extremely small due to compression and distortion, and the accuracy of the calculations in the distorted area is highly suspect because of possible large errors associated with the finite difference approximations in the extremely deformed regions.

From the Lagrangian formulation, the only way to obtain answers at later times for problems experiencing extreme grid compression and distortion is to rezone the computational grid. Basically, a new, undistorted grid is overlayed on the old, distorted mesh. Once the geometric overlay is completed, the physical properties of the new cells are computed from the partial zone properties of the old lattice, assuring that mass, momentum, and energy are conserved. Care must be taken to obtain the new mesh. Essentially, the procedure requires deciding which points need to be moved to make the grid more regular, and then moving these points to new locations. For large problems, even with semi-automatic help from the computer, this can be very tedious and time-consuming. Material regions should not overlap in a new cell (or else the material boundary is destroyed); cells can only exist in material regions; i.e., a cell cannot pass over a free surface, otherwise, for example, conservation of mass would be violated if the material density is held constant. And, usually, the physics which caused the distortion is still manifested in the problem--the newly rezoned grid will become distorted and must be rezoned again. To advance the problem in time may thus require that the rezoning process be performed again and again.

The problems which can be encountered in the Lagrangian calculations because of compression or severe distortion of the grid are alleviated in the Eulerian description because of its fixed grid system. In principle, all hydrodynamic problems could be solved numerically by using a multi-material Eulerian calculation which computes the mass, momentum, and energy flows across the fixed cell boundaries. Turbulent flow, rotational flow, high velocity impacts, highly compressed states, etc., can be computed using a Eulerian computer code. Diffusion and the mixing of gases can be handled by an Eulerian description. (Because each cell in a Lagrangian description is uniquely one material, and flow across cell boundaries is not allowed, diffusion and mixing problems cannot be analyzed with a Lagrangian code.) As already stated, a mesh must first be generated; this mesh must be large enough to contain all of the physical space in which action may occur. Cells must be present in the Eulerian grid to catch the flow of mass, momentum, and energy into initially unoccupied regions.

Most of the current codes, while allowing as many as nine distinct materials in the computational grid, restrict a particular cell to a maximum of two materials, though recent work has expanded this to four or more materials (W. Johnson, 1986; Thompson, 1986). (This constraint was the result of bookkeeping on the part of the code, and was a reflection of the needs of users--there had been no significant demand, until recently, for requiring three or more different materials within the same cell.) The collapse and formation of a shaped charge, and the dynamics of high velocity impacts, are typically treated with an Eulerian code.

However, because the Eulerian description describes only what is crossing grid boundaries, the position of lines which approximate material interfaces and exterior boundaries is difficult to determine. The curves which approximate the boundary and material interfaces must move with the material, and consequently will become irregular, time-dependent lines in a fixed Eulerian mesh. Typically, they are known only within the dimensions of a Eulerian cell. In a typical Eulerian hydrocode, interfaces and boundaries are designated by mixed cells, i.e., cells with two materials. Figure 2 depicts an impact between two materials in Eulerian coordinates. At some time $t > 0$, the placement of materials might look like Fig. 2b; mixed cells (whether they be void and material, or materials 1 and 2) are denoted by the "M". The finer the mesh, the more accurately the boundary is represented, but at the price of more computational zones. The

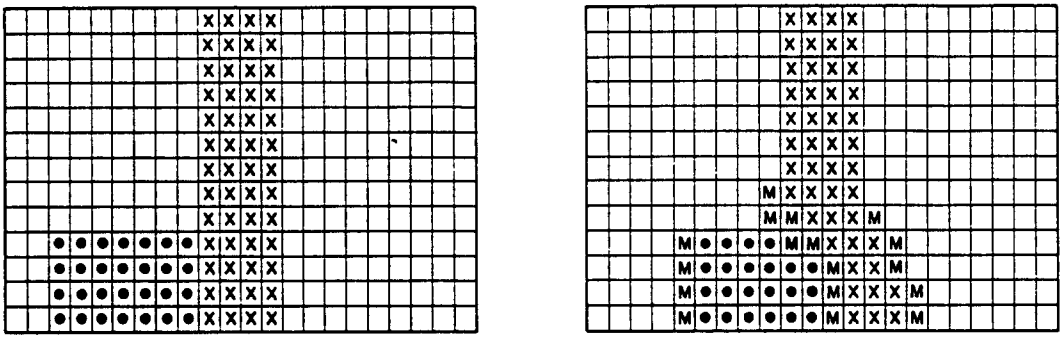

(a.) t = 0 (b.) t > 0

Fig. 2. Eulerian grid with two materials denoted by dots and crosses; "M" denotes mixed cells.

numerical approximation of the differential equations in these irregular boundary cells are not to the same degree of accuracy as interior cells of the mesh. Thus, the application of boundary conditions is generally more difficult and less accurate than for the Lagrangian description.

There is a tendency in the numerical Eulerian formulation for the materials to diffuse across material interfaces at nonphysical rates (because once a material has entered a zone, it is considered to be everywhere in that zone.) This is particularly true when the problem is being carried to long times to find the ultimate configuration or state of the system after most or all external forces have been removed. A finer spaced grid, that is, more zones, can diminish this numerically induced material diffusion, but again at the expense of more computation time. This numerical diffusion problem can be quite severe. The method most commonly used to limit numerical diffusion is one which preferentially transports material out of a cell according to the material contained in neighboring cells. The fraction of each species in a zone is known, and species "a" will be given preference to move into a neighboring cell if the neighboring cell consists mostly of species "a," etc. A procedure for limiting numerical diffusion is required or else the number of mixed zones continues to grow, thereby smearing the interface between the materials. Also, in Eulerian codes, materials are in pressure equilibrium in mixed zones, which requires some sort of iterative procedure between the equations of state of the materials. Thus, the more mixed zones, the more the computational burden.

The Eulerian description describes the instantaneous state of the material in the zone, but has no history of this material. Because the Eulerian description tracks only what crosses cell boundaries, it cannot compute the time history of a particular material particle, which can be important in formulating realistic constitutive, fracture, and failure relations. At the expense of more computational time, "internal state" variables can be devised to transport history dependent variables, though mixing of these variables diminishes their accuracy.

The advantages and disadvantages of the two mathematical schemes can now be summarized. In a Lagrangian calculation, the grid mesh is required only when there is material. The Lagrangian description allows the mesh to be placed such that maximum resolution is obtained for a specific number of zones. Figure 3 depicts a Eulerian grid for the same impact problem of Fig. 1. Figure 3a depicts the grid geometry with approximately the same number zones as shown in Fig. 1, and Fig. 3b depicts the same problem, but with the same spatial resolution (i.e., same zone size). In addition, the Lagrangian grid clearly defines material interfaces and boundaries--their treatment is straightforward. Material and failure modeling can account for rate and history effects. But, as demonstrated in Fig. 1c, the Lagrangian mesh can become severely compressed and distorted which causes the time step to become extremely small, effectively terminating the problem. Also, the numerical differencing schemes become very inaccurate in regions of extreme grid distortion, thus yielding computed quantities that may have little to do with reality. The Lagrangian grid can be rezoned, but in the area where large distortions have occurred, rezoning is akin to an Eulerian calculation.

SPACE DISCRETIZING, TIME INTEGRATION, ACCURACY, AND STABILITY

Although Eqs. (1-7) describe a continuum, the computer is finite. Somehow the problem must be discretized, and then the computer solves these discretized equations. So, the question becomes, how can we best describe or approximate the differential equations describing a continuum with a

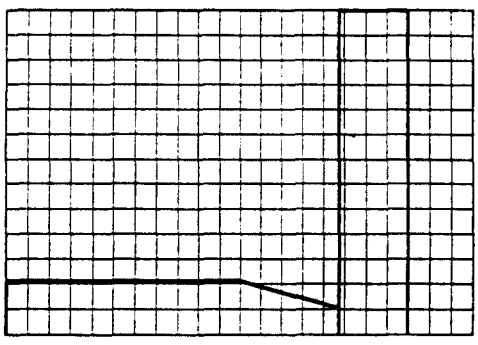

286 Zones

a. Same spatial resolution as Fig. 1.

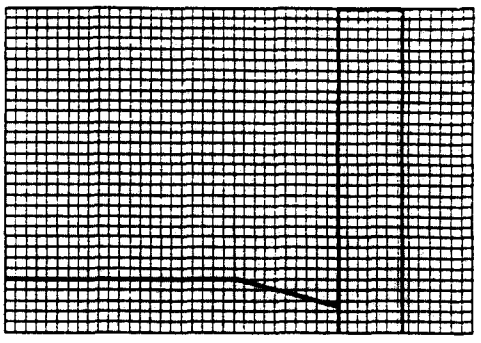

1395 Zones

b. Same number of zones as Fig. 1.

Fig. 3. Comparison of mesh efficiency.

finite and discrete number of points in a computer? A brief overview of the issues in answering this question gives considerable insight to the general features of all hydrocodes, and reasons for the specific algorithms used.

Space Discretization

Two methods for solving continuum problems on the computer are used, finite difference and finite element. Finite element methodology will be discussed later. In the finite difference representation, a lattice of points, or grid, is generated to approximate the geometry of interest. The spatial derivatives in the differential equations are replaced by difference equations, e.g., for some functional F, the partial derivative $\partial F/\partial x$ becomes $\Delta F/\Delta x$ where the differences are computed from values at grid points. The finite differencing is a pointwise approximation. The values computed at a point are then taken to represent the physical parameter over some finite region of space, e.g., a grid cell.

Figure 4a depicts the continuous function F as a function of the spatial coordinate x. By dividing the x-internal into discrete intervals of Δx, the function F at the point $x_n = n\Delta x$ is represented by F_n. The first derivative of F at x_n can be represented by a variety of difference formulas, e.g.,

$$\left.\frac{\partial F}{\partial x}\right|_{x_n} = \frac{F_{n+1} - F_n}{\Delta x} \; ; \qquad \left.\frac{\partial F}{\partial x}\right|_{x_n} = \frac{F_n - F_{n-1}}{\Delta x} \; ; \qquad \left.\frac{\partial F}{\partial x}\right|_{x_n} = \frac{F_{n+1} - F_{n-1}}{2(\Delta x)} \tag{8}$$

which corresponds, respectively, to forward, backward, and central difference equations. Which of these difference formulas, or alternative difference formulas, is the best approximation of the derivative is not as straightforward as one might suppose.

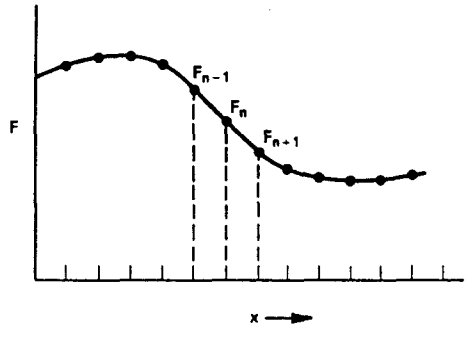

a. Smooth function.

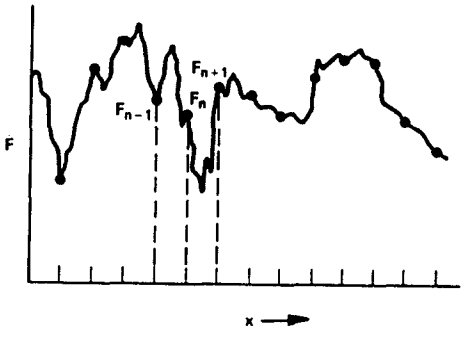

b. Rapidly varying function.

Fig. 4. Space descritization

Time Integration

Several alternatives exist for advancing the solution in time, and just as there is a concern for accuracy in the spatial discretization, the same concern also applies to time integration. The time derivative can be replaced by a difference equation; however, as the solution is advanced in time, the terminology generally used is to refer to the time integration of the differential equations.

Starting at time t^{ℓ}, the solution is advanced by an increment of time Δt to $t^{\ell+1}$ ($t^{\ell+1} - t^{\ell} = \Delta t$).
Equations (1-3, 6) can be written in the general form:

$$\frac{\partial U}{\partial t} = - \frac{\partial}{\partial x} F(U) \equiv G(U) \tag{9}$$

The Mean Value Theorem states that over the interval $[t^{\ell}, t^{\ell+1}]$, there exists some mean value or average G, called $\bar{G}$, which is given by (Hildebrand, 1962):

$$\bar{G} = \frac{1}{\Delta t} \int_{t^{\ell}}^{t^{\ell+1}} G(\tau) d\tau \tag{10}$$

$\bar{G}$ can be computed from known values of G at times t^{ℓ} and $t^{\ell+1}$:

$$\bar{G} = \varepsilon G^{\ell+1} + (1-\varepsilon) G^{\ell} \tag{11}$$

where ε has some value between 0 and 1. Integrating Eq. (9) and using the Mean Value Theorem gives:

$$U^{\ell+1} = U^{\ell} + \Delta t(\varepsilon G^{\ell+1} + (1-\varepsilon) G^{\ell}) \tag{12}$$

Equation (12) is called an implicit integration scheme for any $\varepsilon \neq 0$, meaning that the computed value depends upon both the new and current values of the parameters. As there are N grid points, there are N equations for the N unknowns of each variable. As the equations are nonlinear, an iterative procedure is required to determine the solution at the new time.

By choosing $\varepsilon = 0$, the variables at time $(\ell+1)$ are found directly from parameters already known at time ℓ. The procedure whereby functions at the new time step are determined from the known functions at a previous time step is called an explicit integration scheme. Explicit time integration is used in hydrocodes; the reason for this will be given later.

Criteria for Discretization

There are four properties to be asked of a particular difference representation in order to ascertain the "best" approximation of the differential equations: consistency, accuracy, stability and efficiency. Each of these will be discussed.

Consistency: The first property to be demanded of a difference technique is that the difference equations in some manner approximate the differential equations they are replacing. Formally, it is required that the difference scheme reduce to the differential equation in the limit as Δt and Δx go to zero; e.g., $\lim (\Delta F/\Delta x)\ \Delta x \to 0\ \partial F/\partial x$. This requirement is fundamental, otherwise the difference scheme does not simulate the differential equation (e.g., Lax and Richtmyer, 1956). However, the use of finite spatial and time steps produces errors and makes the solution deviate from the solution to the differential equation; thus, the difference solution must be examined in more detail.

Accuracy: Two types of errors occur which impair the accuracy of a difference scheme, round-off errors and truncation errors. Round-off errors are associated with the precision of the computer, that is, the number of significant digits carried by the computer to represent a variable. Scientific computers represent each number with 60 to 64 bits called a word, which permits the retention of approximately fourteen to eighteen "significant" digits. Variables, such as pressure, will change by many orders of magnitude in a dynamic shock event simulated by hydrocodes. Additionally, a large number of cycles are executed to advance the solution in time. These two factors require that a large number of digits be carried by the computer. These "significant" digits are not carried to increase the accuracy of an answer by giving more significant digits per se (often, the input parameters may not be known to more than two or three significant digits, so the final answer cannot be more accurate than the input), but rather, to minimize round-off errors. Even with the large number of computer digits, occasions do arise where round-off errors create difficulties. Sometimes, special algorithms are necessary to handle certain types of round-off errors.

A second type of error is the result of the approximation scheme used, and is called truncation error. The essence of this error arises from representing a continuous variable with a discrete number of points, and the magnitude of the errors depends on the mesh intervals in time and space. Taylor series expansion provides a means to estimate the truncation errors in representing derivatives with difference equations. For example, the backward difference and forward difference schemes for $\partial F/\partial x$ ignored terms of the order (Δx) and higher; whereas, the central difference scheme ignored terms of the order of $(\Delta x)^2$. These difference schemes are referred to as first-order accurate, and second-order accurate, respectively. Since any spatial interval can be normalized to run from x=0 to x=1, it is clear that difference schemes with truncation errors of $(\Delta x)^2$ are more accurate than first-order accurate difference equations. However, because of stability issues, an alternate method for estimating accuracy will be discussed.

J. von Neumann developed an analysis procedure for analyzing the frequency response of finite difference equations with respect to both accuracy and stability (von Neumann and Richtmyer, 1950; Richtmyer and Morton, 1967). Consider a problem in one-dimension whose solution is given by a continuous function F(x) on the interval $0 \leq x \leq L$. The solution can be written as a Fourier series:

$$F(x) = \sum_{k=-\infty}^{\infty} g_k e^{i\pi kx/L} \qquad g_k = \frac{1}{L} \int_0^L F(x)\, e^{-i\pi kx/L} dx \tag{13}$$

On the computer, a discrete number of points N is used to represent the function. Thus, the infinite sum given in Eq. (13) is replaced by a finite series. The spacing between grid points (assumed here to be constant) is Δx; thus, the total length of the interval is given by $L = N(\Delta x)$, and x by $n(\Delta x)$. Hence, the function at the n-th grid point is given by:

$$F_n = \sum_{k=1}^{N} g_k\, e^{ik\pi n/N} \qquad g_k = \frac{1}{N} \sum_{k=1}^{N} F_n\, e^{-i\pi kn/N} \tag{14}$$

Wavelengths go from a minimum of $2(\Delta x)$ to a maximum of $2N(\Delta x)$. No wavelengths shorter than $2(\Delta x)$ can be defined on the spatial mesh. Thus, if the function "wiggles" in an interval shorter than Δx, there is no way to resolve these "wiggles." This is depicted in Fig. 4b. In order to resolve a rapidly varying function, more points are required on the interval. The greater number of points implies a larger N and smaller Δx. The effect in terms of wavelength is that by decreasing Δx, the spatial grid has an improved frequency response.

In using these Fourier modes, an estimate of the accuracy of the finite-difference scheme can be made. For example, the central difference scheme, Eq. (8c) gives the following (Potter, 1973):

$$\Delta_n' = \left(1 - \frac{k^2(\Delta x)^2}{6} + O[(\Delta x)^4]\right) \frac{\partial}{\partial x} \tag{15}$$

where the Δ'_n is the difference operator. Thus, the difference operator is equal to the partial derivative within a factor of $(\Delta x)^2$, i.e., second-order accurate. However, the real importance of using Fourier modes is in the investigation of numerical stability.

Lax-Wendroff Method: From 1960 through the mid 70's, a number of investigators searched for the "best" difference representation of the continuum equations. Much of this research is documented in the Journal of Computational Physics, though considerable "testing" and comparison of the various schemes were performed at different Government laboratories and universities. In this search for an accurate simulation of the difference equations, Lax and Wendroff (1960) devised an integration scheme that used a difference representation developed by Lax (1954). Richtmyer and Morton (1967) simplified the scheme somewhat by rewriting the original Lax-Wendroff method as a two-step method.

Consider the general advection equation, Eq. (9). By computing variables at a time $t^{\ell+\frac{1}{2}}$ and half-way between grid points, $n+\frac{1}{2}$, the difference equations become second-order accurate in both time and space.

This scheme is depicted in a space-time difference mesh in Fig. 5. In essence, the two-step Lax-Wendroff method is a predictor-corrector method. The first step predicts the values of U at the half-time, half-space points:

$$U_{n+\frac{1}{2}}^{\ell+\frac{1}{2}} = \tfrac{1}{2}(U_n^{\ell} + U_{n+1}^{\ell}) - \frac{\Delta t}{2(\Delta x)} \left(F_{n+1}^{\ell} - F_n^{\ell}\right) \tag{16}$$

and then these values of U define the fluxes at the intermediate time and space points:

$$F^{\ell+\frac{1}{2}}_{n+\frac{1}{2}} = F(U^{\ell+\frac{1}{2}}_{n+\frac{1}{2}}) \qquad (17)$$

The corrector step computes U at the final time for each spatial grid point:

$$U^{\ell+1}_{n} = U^{\ell}_{n} - \frac{\Delta t}{\Delta x}\left(F^{\ell+\frac{1}{2}}_{n+\frac{1}{2}} - F^{\ell+\frac{1}{2}}_{n-\frac{1}{2}}\right) \qquad (18)$$

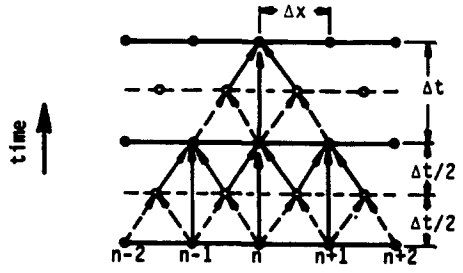

Fig. 5. Lax-Wendroff method.

While no hydrocode may explicitly use the Lax-Wendroff method, the essence of the method is used by most of the codes. In particular, by defining cell-centered quantities for the stresses (and pressures), densities, and internal energies, the velocities at each grid point are computed at $t^{\ell+\frac{1}{2}}$. Then these velocities are used to advance the cell-centered variables to $t^{\ell+1}$.

Conservation on a Difference Mesh: The system of partial differential equations is nonlinear, and in defining a particular difference method, there are a variety of ways of differencing the nonlinear terms. When nonlinear terms are present, the difference methods do not have the same accuracy for all terms. The effect is to have local sources and sinks of mass, momentum and energy (Emery, 1967). These anomalies are most often manifested in the presence of strong pressure gradients (shocks). Since Eqs. (1-3) were derived from application of conservation of mass, momentum and energy, it would seem natural to ask if the difference equations also could be conservative. Lax and Wendroff (1960) showed that if the hydrodynamic equations could be put in the form (Richtmyer and Morton, 1967; Roache, 1972):

$$\frac{\partial U}{\partial t} + \frac{\partial}{\partial x} F(U) = 0 \qquad U = \begin{pmatrix} \rho \\ \rho U \\ e \end{pmatrix} \qquad F(U) = \begin{pmatrix} \rho U \\ \rho U^2 + P \\ (e+P)U \end{pmatrix} \qquad (19)$$

then the difference equations are conservative. Both the Eulerian and Lagrangian descriptions can be put in a conservative form (Richtmyer and Morton, 1967). The implication is that the difference scheme, independent of truncation errors, will identically conserve mass, momentum and energy (except for round-off errors).

Stability: Unfortunately, answering the question of accuracy is not sufficient--certain difference schemes lead to numerical instabilities (for example, see Walsh, 1972). If the difference scheme produces a solution which is not bounded, the scheme is said to be numerically unstable. A numerical method is stable if a small error at any stage produces a smaller cumulative error. If an error is amplified from time step to time step, the error will quickly swamp the solution and the result will be meaningless. For example, assume that an error ε exists in the parameter U at time step ℓ. The calculation of the U at time step $(\ell+1)$ will have an error associated with it, and both $U^{\ell+1}$ and $\varepsilon^{\ell+1}$ will be functions of U and ε at the previous time steps:

$$U^{\ell+1}_{n} + \varepsilon^{\ell+1}_{n} = f(U^{\ell}_{n} + \varepsilon^{\ell}_{n}) \qquad (20)$$

The amplification of the error at time step $(\ell+1)$ is given by:

$$\varepsilon^{\ell+1} = g\,\varepsilon^{\ell} \qquad (21)$$

where "g" is termed the amplification factor. This amplification factor is related to truncation errors and the integration schemes used, but is not associated with round-off errors. For stability, the requirement is that the error at time $(\ell+1)$ be less than or equal to the error at time ℓ, otherwise the error will grow as time increases. This leads to the very important conclusion: the absolute magnitude of the amplification factor must be less than or equal to one for a numerical scheme to be stable:

$$|g| \leq 1 \qquad \text{for stability} \qquad (22)$$

In general, a whole system of difference equations exists (at least one for each grid point); the amplification factor is a tensor, and the errors can be represented as components of a multi-element vector (Richtmyer and Morton, 1967). However, the conclusion of Eq. (22) remains the same except that the condition for stability must be applied separately to the amplitude of each

error eigenvector. In general, the eigenvalues of the amplification matrix may be complex, in which case the magnitude of the amplitude is given by $[g^*g]^{\frac{1}{2}}$, where g^* is the complex conjugate of g.

The errors in Eq. (20) also satisfy the general partial differential equations. Separation of variables is used to separate the time component of ε from the spatial component:

$$\varepsilon = \varepsilon^*(t)e^{ikx} \tag{23}$$

where $\varepsilon^*(t)$ gives the amplitude of the Fourier mode. As any waveform can be approximated by the superposition of the various wavelengths in a Fourier series, then the procedure is to demand stability for an arbitrary wavelength, represented by the wavenumber k. Application of the von Neumann stability methodology to the Lax-Wendroff method yields for the amplification matrix (Richtmyer and Morton, 1967):

$$g = 1 - i\alpha\sin(k\Delta x) - \alpha^2[1 - \cos(k\Delta x)] \qquad \alpha = \frac{c\Delta t}{\Delta x} \tag{24}$$

$$g^*g = 1 - \alpha^2 (1 - \alpha^2) [1 - \cos(k\Delta x)]^2 \tag{25}$$

where c is the wave speed. The requirement that $[g^*g]^{\frac{1}{2}}$ be less than or equal to one, for all k, gives the famous Courant-Friedrichs-Lewy (CFL) stability condition (Courant, et al., 1928):

$$\alpha \leq 1 \qquad \text{i.e.,} \quad \frac{c\Delta t}{\Delta x} \leq 1 \quad \text{or} \quad \Delta t \leq \frac{\Delta x}{c} \tag{26}$$

Equation (26) is for Lagrangian coordinates; in Eulerian coordinates, the sound speed is replaced by the sum of the particle velocity and sound speed:

$$\Delta t \leq \frac{\Delta x}{|v| + c} \tag{27}$$

The stability criterion is essentially a statement of casualty, i.e., no signal (information) can be allowed to propagate across the shortest dimension of a zone in a time Δt. Though the CFL criterion was found here for the Lax-Wendroff method, it applies equally to other stable difference representations. (Some difference representations lead to an amplification matrix which gives $|g| > 1$ for any value of Δt.)

It is worth remarking here that for small wave numbers ($k\Delta x$ small), the cosine in Eq. (25) can be expanded in a Taylor series to yield:

$$g^*g = 1 - \alpha^2(1 - \alpha^2) \frac{k^4(\Delta x)^4}{4} + O(k^6(\Delta x)^6) \tag{28}$$

Thus, numerical diffusion, i.e., the smearing of a variable over space, occurs only to the fourth order in the wave number (Potter, 1973). Long wavelengths are only minimally affected, while the effect of fourth-order diffusion tends to smooth short wavelength discontinuities on the difference mesh (see the section on artificial viscosity in this paper). Additionally, because there is no imaginary component in Eq. (28), no unwanted oscillations appear in the solution. These features, in addition to being second-order accurate in the spatial derivative and time integration, have lead to wide application of the Lax-Wendroff method.

Efficiency: The last requirement for a numerical technique is efficiency. A computer is finite; only so much memory is available, and the calculation time required to get a numerical solution must be reasonable. For many computer systems, the costs of running a problem are related to central processing time, memory requirements, and input/output operations. The efficiency of a particular numerical scheme can be defined as the total number of arithmetical, logical, and storage operations performed by the computer to obtain a solution over a unit time-length of the problem. Efficiency decreases with greater complexity of the numerical technique; however, the accuracy of the numerical solution is generally increased with increasing complexity. In a hydrocode, several thousands of variables typically are computed for each time step. It is important that the numerical differencing and integration technique be as efficient as possible; but at the same time, for the solution to be of any value, the numerical techniques must be accurate. A compromise must be reached between efficiency and accuracy. It has been found that the small grid sizes necessary to resolve important shock interactions give quite accurate results using second-order accurate methods (Herrmann, 1977). The increased complexity and extra computations necessary to go to higher order methods, even with some attendant increase in grid size, appear to be computationally inefficient.

Finite Element Discretization

Whereas the finite difference technique is a pointwise discretization of the continuum, finite element techniques envision the solution region as being composed of many small interconnected sub-regions or elements. Thus, a piecewise approximation of the differential equations is made. Nodes are assigned to elements and then an interpolating function, typically a polynomial (a spline function is another possibility), is used to represent the variation of the variable over the element.

The degree of the polynomial is related to the number of nodes and degrees of freedom of the nodes in the element. The displacements at these nodal points are the basic unknowns of the problem. These displacement functions define a state of strain and strain rate within each element; with the constitutive equation, the state of stress is determined. The forces, concentrated at the nodes, relate internal loads, external loads, and the nodal displacements. The total potential energy is found, then variational calculus is used to minimize the potential with respect to the coefficients of the polynomials, resulting in a system of algebraic equations for the unknown coefficients.

Traditionally, finite element formulations have inverted the so-called stiffness matrix. An iterative scheme is then required to obtain the solution. For dynamic, time-dependent problems, Belytschko recognized that the stiffness matrix was in fact unnecessary for the explicitly integrated finite element methods (Chiapetta, Belytschko and Rouse, 1973; Belytschko, Chiapetta and Bartel, 1976; Belytschko, 1976). Thus, the finite element hydrocodes are integrated directly. The first adaptation of an explicit time integration scheme to a large deformation finite element code which also could handle shocks was HONDO (Key, 1974; Key, 1974b; Key, et al., 1978). Independent work by Johnson (1976, 1977, 1977b, 1977c, 1982), and by Hallquist (1976; 1976b; 1978; Goudreau and Hallquist, 1982) has led to the EPIC and DYNA families of codes, respectively. These last two families of codes are used extensively to solve shock propagation problems.

In summary, Gordon Johnson has described the difference between the two techniques as, "Finite difference techniques are an approximate solution to an exact problem, and finite element techniques are an exact solution of an approximate problem." There is no basic mathematical difference between the two methods; Belytschko (1976) has shown that the discrete forms of the equations of motion of the finite element are equivalent to those of the finite difference method for a number of cases. The differences are in the implementation.

Finite element codes, by the nature of their formulation, automatically incorporate certain types of boundary conditions. The equations of motion are formulated through nodal forces for each element, and do not depend on the shape of the neighboring mesh. Equations of motion in the finite difference method, on the other hand, are expressed directly in terms of the stress gradients of the neighboring grid.

Historically, a criticism of the finite difference technique was that it could not represent an irregular surface; finite elements were noted for their ability to handle complicated geometries. Conversely, finite element techniques have been criticized for their poor constitutive capabilities and the lack of capabilities seen in some finite difference codes, e.g., slidelines, rezoning, etc., (Belytschko, 1976). However, these criticisms are no longer applicable. Mesh generator schemes in finite difference codes have become fairly sophisticated; and slidelines, and material libraries with attendant constitutive models have become very much a part of finite element hydrocodes. The large difference between the finite element and finite difference techniques has closed considerably, and perhaps the best way of summarizing is to say that the two techniques provide different algorithms for obtaining solutions to the same differential equations.

The four properties of the discretization process (consistency, accuracy, stability, and efficiency) apply equally to the finite element process, though the explicit implementation might vary in comparison with finite difference techniques. For example, consistency is automatically implied by the minimization technique. Accuracy is just as relevant to finite elements as finite difference. Large zone sizes can be accomplished by going to higher order elements, i.e., using quadratic and cubic polynomials (akin to going to higher order difference approximations). In finite element hydrocodes, the complexity of using higher order elements versus resolution of wave interactions is not warranted (efficiency), and constant stress elements are typically employed. Stability criteria, which result from separating the spatial and time discretization process, apply equally as well to finite element. The CFL condition holds for constant stress elements, and perhaps a more severe restriction holds if higher order elements are used. And, finally, since the mesh size in both finite difference and finite elements are considerably larger than the thickness of the shock, both techniques require artificial viscosity so that the same equations will handle the propagation of shocks. This is the topic of the next section.

TREATMENT OF SHOCKS

The discussion to this point has been concerned with the field equations where it has been assumed that the physical variables of interest vary smoothly enough that they can be resolved on a finite difference or finite element grid. We already have discussed that a complex waveform can be reconstructed from an infinite number of terms in a Fourier series. However, wavelengths smaller than the grid spacing cannot be described, thus limiting the grid's ability to resolve physical phenomena which may be occurring very rapidly. Shocks, on the other hand, can be described by an instantaneous jump in the velocity, pressure, and density. At first glance, it would appear that a finite difference representation of the continuum equations would not permit a calculation involving the propagation of shocks. However, two approaches exist for the calculation of problems containing shocks.

One approach is to use the Rankine-Hugoniot jump conditions. This approach generally is combined with the mathematical technique called method of characteristics. In a sense, information flows along the characteristics which move at the wave speed. This method is excellent for understanding the detailed wave motion; however, if the ultimate state of the material is desired, a finite-difference code is generally superior (Karpp, 1972).

The second approach is to use the discretization procedure on the differential equations. But the equations must be modified slightly in order to obtain any meaningful numerical results. Before discussing the modifications, it is instructive to look at the numerical solution of a shock propagating into steel at two different times, Fig. 6, using the Lax-Wendroff method. The dots on the figure denote the values of the pressure at the grid points. The dashed line represents the true solution. Large amplitude oscillations are observed in the numerical solution. These oscillations are not instabilities; a calculation can be continued indefinitely and the amplitude of the oscillations will remain approximately the same. We note here that a Lax-Wendroff scheme was used in Fig. 6, and that if a different finite-difference scheme were used, then the solution might well appear as Fig. 7. (The reason for the marked difference in Figs. 6 and 7 is the result of a dissipation term inherent in the Lax-Wendroff method, which dampens the short wavelength oscillations away from the shock front.) The large oscillations in Figs. 6 and 7 have little to do with the solution to the exact differential equations, and, furthermore, can swamp the true solution.

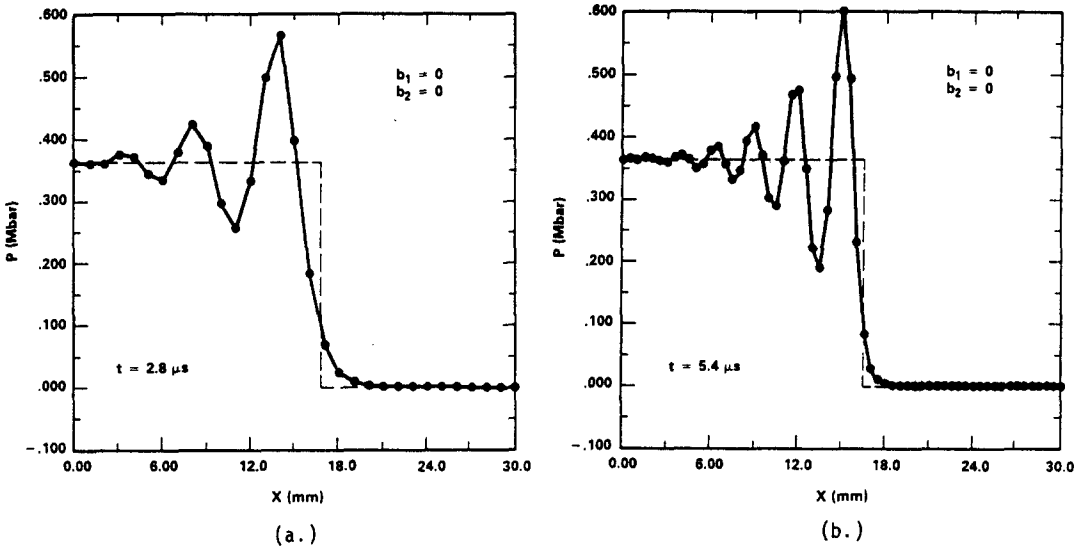

Fig. 6. Shock propagation into steel bar.

Several interpretations have been used to describe physically the oscillations in Figs. 6 and 7. One interpretation by Potter (1973), is that the energy of the large amplitude disturbance tends to aggregate in the shortest wavelengths on a difference mesh (that is, the high frequency components of the Fourier series representation contain the energy). Consequently, the difference solution will induce very large oscillations between the variables on adjacent mesh points. Other interpretations also have been given (Richtmyer and Morton, 1967). Regardless of the interpretation, the "excess" energy manifested in the large amplitude variations needs to be converted to a true internal energy.

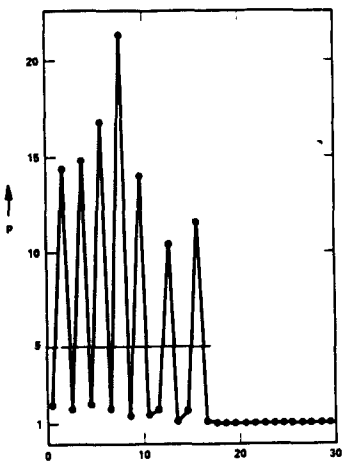

Fig. 7. An alternate differencing scheme (from Richtmyer and Morton, 1967).

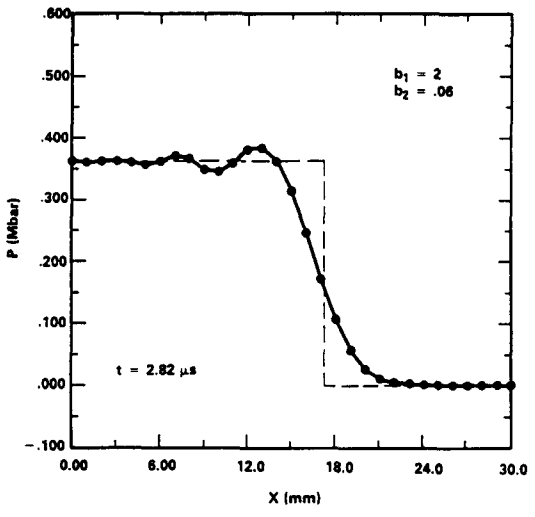

Fig. 8. Shock propagating into steel bar, with artificial viscosity.

Artificial Viscosity

Von Neumann and Richtmyer (1950) devised a method for handling shocks by introducing a purely artificial dissipative mechanism. Physical insight suggested this type of formulation. Becker (1922) had studied the effect of heat conduction and viscosity on shocks. As reported in Richtmyer and Morton (1967):

> He [Becker] showed that, when heat conduction is allowed for, the temperature varies smoothly through the shock layer and that for shocks of strength less than a critical value, the pressure and density vary smoothly also; whereas, for stronger shocks, the transition of pressure and density from their initial to their final values is partly by a smooth variation and partly by a discontinuous jump. When viscosity is allowed for, however, all quantities vary smoothly through the shock region for a shock of any strength. In either case the thickness of the transition zone is proportional to the coefficient of the dissipative mechanism, so that in the limit of no heat conduction and no viscosity the variations approach the discontinuous ones of the Hugoniot theory.

The idea then was to introduce a dissipative mechanism that would result in the shock being spread smoothly over several mesh intervals. Viscosity is a mechanism which has such a dissipative effect, and certainly appears to be more appropriate than a heat conduction term. The procedure thus required that some artificial viscosity term be devised that had the right strength to spread the shock over several computational zones, and could be incorporated into the difference equations. In traditional fluid mechanics, a viscosity term appears in the one-dimensional momentum equation as:

$$\text{viscosity term: } \frac{\partial}{\partial x}\left(\mu \frac{\partial v}{\partial x}\right) \tag{29}$$

where μ is a coefficient of viscosity. This would suggest that an artificial viscosity term q could be added directly to the pressure in the differential equations, e.g., $\partial(p+q)/\partial x$, where q is called the artificial viscosity and would be of the form $\mu \partial v/\partial x$.

Becker had shown that with ordinary viscosity, in which the stress is proportional to the rate of shear and is represented by a linear term in the velocity, the thickness of the transition layer varies with the shock strength, approaching zero for very strong shocks and infinity for very weak shocks. In their original formulations, von Neumann and Richtmyer were concerned that the thickness of the shock should be independent of the shock strength since this was to be a numerical artifact. Indeed, physical reasoning implied that the strength of the artificial viscosity term would be orders of magnitude larger than real viscous effects, since normally, real viscous effects can be ignored in most treatments of shocks. The form of the artificial viscosity term was chosen as:

$$q_1 = -a_1^2 \rho \left| \frac{\partial v}{\partial x} \right| \frac{\partial v}{\partial x} \tag{30}$$

where a_1 has the dimensions of length. It was later found that a more appropriate expression was:

$$q_1 = \begin{cases} a_1^2 \rho (\partial v/\partial x)^2 & \partial v/\partial x < 0 \\ 0 & \partial v/\partial x \geq 0 \end{cases} \tag{31}$$

that is, the artificial viscosity term need only be present during material compressions. For most problems, either formula is satisfactory because q is extremely small except at the shock front. However, when extreme expansion (as of a free surface) can take place, the second expression is superior (Richtmyer and Morton, 1967). The adjustable constant a_1 can be written as $b_1^2(\Delta x)^2$, thereby making the difference representation of Eq. (31) independent of zone size.

Adding a linear artificial viscosity term, with a_2 a constant with the dimensions of length, and c the sound speed:

$$q_2 = a_2 c \rho \frac{\partial v}{\partial x} \tag{32}$$

has the advantage of further smoothing the oscillations not totally dampened by the quadratic artificial viscosity term. The constant a_2 can be defined as $b_2(\Delta x)$ to keep the difference representation independent of mesh size. Greater care must be exercised with the magnitude of b_2 since there is a much greater chance of distorting the solution away from the shock.

Figure 8 shows the numerical shock profile at the same time as Fig. 6b, but with both the quadratic and linear artificial viscosity terms present. The choice of the constants b_1 and b_2 determine the number of zones over which the shock front is smeared, versus the oscillations behind the front. In Figure 8, the shock front is smeared over approximately eight zones; the front could be steepened if finer zoning was used.

Shock Viscosity

Notwithstanding that code results are often in excellent agreement with experiments, researchers were not necessarily happy with the concept of artificial viscosity, but rationalized its use as a practical substitute for real viscous processes. But a very significant finding by Swegle and Grady (1985) has altered the above objection. Figure 9 is a plot of the Hugoniot stress σ_H, versus the maximum strain rate $\dot{\epsilon}_m$, for a number of different materials. Note that all materials have essentially the same slope. From Fig. 9, the maximum strain rate can be written as:

$$\dot{\epsilon}_m = A \sigma_H^4 \tag{33}$$

where A is the intercept, a material dependent parameter. Whereas the artificial viscosity is proportional to sum of the strain rate and the square of the strain rate, the actual viscosity in the shock front is proportional to the strain rate to the one-fourth power.

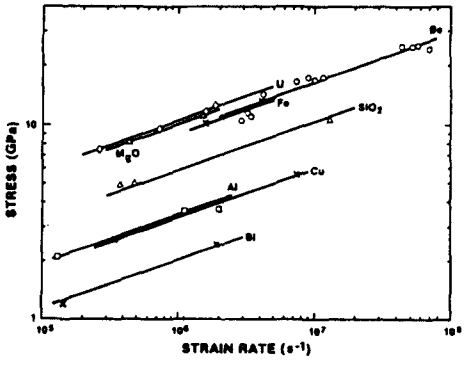

Fig. 9. Maximum shock stress versus strain rate (from Swegle and Grady, 1985).

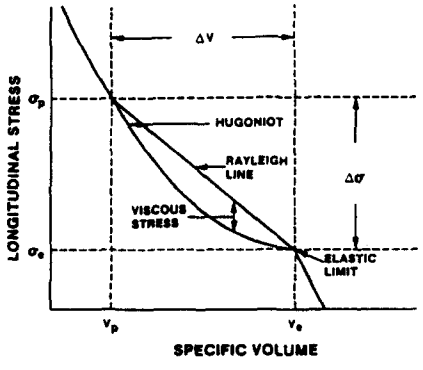

Fig. 10. Schematic for viscous stress (from Swegle and Grady, 1985).

It is assumed that the viscous stress is a purely deviatoric stress (there is no bulk viscosity), and that this viscous stress, τ_v, can be identified as the stress on the Rayleigh line minus the equilibrium stress, taken to be the Hugoniot, Fig. 10. Swegle and Grady show that the differential change in the octahedral shear stress τ, is a function of both total strain rate $\dot{\varepsilon}$, and the viscous stress τ_v:

$$d\tau = 2G\dot{\varepsilon}dt - 2GA'\tau_v^2 dt \qquad A' = 8\sqrt{2}\,\rho_e^2 c_o^4 A/3s^2 \tag{34}$$

where G is the shear modulus, and A' is a constant which incorporates the material properties of Fig. 9; ρ_e is the density at the Hugoniot elastic limit, c_o is the bulk sound speed, s is the slope in the linear shock-particle velocity relationship, and A the intercept from Fig. 9.

Normally, for an elastic, perfectly plastic material, the material state point is calculated assuming that the current strain increment is strictly elastic (Wilkins, 1964). If the resulting state point lies outside the von Mises yield surface, then the stresses are adjusted radially to bring the state point back to the yield surface. But now, the difference in the stress at the "elastic" state point, computed from the first term of Eq. (34a), and the yield surface is assumed to be the viscous stress. The stress is then relaxed by the second term in Eq. (34a), which is proportional to the square of the viscosity. Subcycling on the timestep is required to insure that the finite difference expression for Eq. (34a) is an accurate solution of the differential equation (otherwise, the stress setback could exceed the first term, and the stress state would lie inside the yield surface).

With this technique, shocks have a finite rise time and thus a finite thickness. The thickness of the shock front is given by the material parameter A' of Eq. (34b). Of course, the computational zone size must be sufficiently small to resolve the details of the shock front. Figure 11 shows comparison between experiment and the hydrocode calculations for copper at two different shock amplitudes. These hydrocode calculations were performed without any artificial viscosity. A zone size of 10^{-5} to 10^{-4} cm, depending upon the shock strength, is required to resolve the shock front.[1] Swegle and Grady report that if the zoning is too coarse for the given problem, the solution becomes very noisy, i.e., if the grid size cannot resolve the shock, then standard artificial viscosity methods must be used to spread the shock over several computational zones.

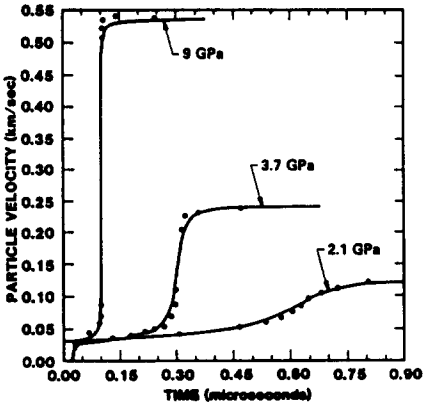

Fig. 11. Comparison of experiment (dotted line) and calculation (solid line) wave profiles for aluminum (Swegle and Grady, 1986).

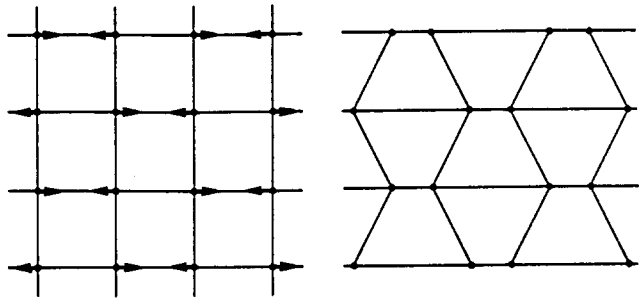

(a.) Velocity Field (b.) Deformation

Fig. 12. Keystone velocity field and deformation.

[1] Walsh and Tillotson (1963), using a qualitative argument, point out that data (Eichelberger and Gehring, 1962) for crater depth show simple linear scaling. The validity of simple linear scaling follows directly from Rankine-Hugoniot and continuous hydrodynamic flow equations which are homogeneous in the space and time variables. This is true only if thermal conduction and viscous effects are negligible; otherwise, second derivatives enter the equations and the scaling no longer applies. Since the experimental data used projectiles with dimensions from 10^{-4} cm up to 10 cm, the conclusion was that it was appropriate to neglect viscosity effects for dimensions larger than 10^{-4} cm. It is interesting to speculate that if Eichelberger and Gehring had been able to fire slightly smaller projectiles (which already were on the order of 10^{-11} gm), and taken measurements, that the effects of shock front viscosity might have been evident.

Obviously, this very, very small zone size is unacceptable in many applications; nevertheless, the model permits the calculation of the correct strain rates in the shock front. The development of micromechanical models in which the evolution of parameters is controlled by the strain rate, such as adiabatic shear instabilities, can now be investigated at a more fundamental level. If the details of the shock front are not important, or are of secondary importance, then the usual artificial viscosity methods should be used.

Keystone Viscosity

A common numerical phenomena observed in dynamically loading, e.g., impact, is the situation where the velocities of the mesh points on opposite corners of the mesh are equal, Fig. 12a. This velocity field produces no strain or volume change in the mesh since the finite difference equations for the components of the strain rate tensor involve velocity differencing of the grid points. The stress and viscosity components are all zero and there is no resistance to the deformation caused by this type of velocity field. In finite element theory, the difficulty arises because of the assumption of a homogeneous strain field which is incompatible with a four sided element (Belytschko, 1974). The grid will take on the characteristic "keystone" appearance shown in Fig. 12b. To control this type of deformation, another type of viscosity is introduced to give artificial rigidity to the mesh, called keystone viscosity or hourglass viscosity. The reader is referred to Swegle (1978) or Belytschko (1984) for appropriate expressions. Care must be exercised with keystone viscosity since it invokes nonphysical restoring forces and thus may produce nonphysical solutions. Typically, the coefficient for keystone viscosity is zero or very small unless the user encounters a situation where the grid is distorting into the keystone appearance.

Stability and the Time Step

Stability has been discussed in some detail earlier in this paper. However, a modification to the CFL stability condition deduced from the simple transport problem, Eq. (26) or (27), has to be made because of artificial viscosity.

Addition of the artificial viscosity to dampen the oscillations resulting from the passage of shocks also limits the time step. When the von Neumann stability method is used on a diffusion-type differential equation (i.e., a parabolic differential equation, whereas the wave equation is a hyperbolic equation), the stability criterion is found to be dependent on the diffusion coefficient. The mathematical treatment is still not understood (Richtmyer and Morton, 1967) and a form of the stability requirement must rely on empiricism; the method employed in the Sandia codes has been found to work well (Kipp and Lawrence 1982; and Swegle 1978):

$$\Delta t \le \frac{\Delta x}{A + [A^2 + c^2]^{\frac{1}{2}}} \qquad A = 2b_1^2 (\Delta x)|\partial v/\partial x| + b_2 c \tag{35}$$

Note that the time step must decrease as the "diffusion" term (related to the artificial viscosity) grows larger. Wilkins (1964), and Richtmyer and Morton (1967) give slightly different expressions. Equation (35) reduces to the familiar CFL condition if the artificial viscosity coefficients are set to zero (as they are during an expansion phase); but the diffusion term controls the time step when it is large, i.e., when shocks are present. For multiple dimensions, the definition of A changes slightly as the quadratic artificial viscosity term is extended to two or three dimensions.

In the section on time integrations, an implicit integration scheme was discussed. If the von Neumann stability analysis is applied to Eq. (12), $\varepsilon \neq 0$, the amplification factor is found to be less than or equal to one for all wave numbers, implying that the implicit integration scheme is unconditionally stable. Thus, the difference equation is numerically stable regardless of the size of the time step, though in practice the time step might be limited by the ability of the convergence scheme to converge to a solution. One might then ask, "Why not use an implicit integration scheme for hydrocodes?" Because shocks travel distances of millimeters per microsecond, the time step must be small to resolve the temporal details. Since the time steps are necessarily limited by the desire to resolve shock wave interactions, the added complexity of an implicit integration scheme, with its attendant number of interactions (and often convergence problems) is not warranted (also, see Herrmann, 1977). In structural response calculations, or heat transfer calculations, significant changes occur over timeframes which are orders of magnitude longer than microseconds, thereby making implicit schemes useful in those problems. Thus, for hydrocode calculations, the time step is limited by the modified Courant condition, Eq. (35).

The time step is dramatically affected by changing the grid size. In one dimension, halving the grid size quadruples the number of computations, since twice as many zones are now involved in the mesh, and by Eq. (26c), the time step has been halved. In two dimensions, doubling the

number of zones in the two dimensions increases the run time by at least a factor of 8 (to reach the same time), while in three dimensions, doubling the number of zones in all directions requires at least 16 times more computational steps.

MATERIAL MODELING IN HYDROCODES

The preceding discussions have dealt solely with how the continuum equations are solved on the computer. Specific material properties govern the response of materials, and result in different behavior for nominally the same impact conditions. Material modeling can be divided into three areas: volumetric response, or resistance to compressibility (equation of state), the resistance to distortion (constitutive); and the reduction in ability to carry stress as damage accumulates (failure). The importance in understanding and modeling material response is reflected in the papers by Asay and Kerley (1986), Holian and Burkett (1986), Kerley (1986), Steinberg (1986), Drumheller (1986), and Trucano and Asay (1986). An excellent monograph by the National Academy of Sciences (1980) reviews the state of understanding of the response of metals to ultra-high loading rates, though with particular application to armor. The following paragraphs summarize material modeling in hydrocodes.

Equation of State

Whether a material has strength or not, some expression is required to express the relationship between pressure, volume, and internal energy. This relationship is called the equation of state. Thermodynamic theory allows a description of a material to be given by three thermodynamic variables, such that one variable can be expressed in terms of the other two, e.g., the pressure in terms of the internal energy E, and specific volume V ($\rho = 1/V$):

$$P = f(E, V) \tag{36}$$

Equation (36) can be thought of as a surface in pressure-energy-volume space. As such, a change in the pressure dP can be written in terms of the changes in the other two variables:

$$dP = \left(\frac{\partial P}{\partial V}\right)_E dV + \left(\frac{\partial P}{\partial E}\right)_V dE \tag{37}$$

where the subscript E and V on the parentheses refer to the derivative being performed with one variable while holding the other constant. Integration of Eq. (37) allows the pressure to be expressed in terms of the volume V and energy E relative to the pressure at a reference energy and volume, E_R and V_R.

The Gruneisen parameter is defined as:

$$\Gamma = V \left(\frac{\partial P}{\partial E}\right)_V \tag{38}$$

and if it assumed that Γ is pressure independent, then it can be shown that the integration of Eq. (37) gives (Rice, et al., 1958; McQueen, et al., 1970):

$$P = P_H(V) + \frac{\Gamma}{V} (E - E_H) \tag{39}$$

where the reference state is taken as the Hugoniot. Equation (39) is referred to as the Mie-Gruneisen equation of state, and it permits the evaluation of the pressure at some volume and energy off the Hugoniot. The Gruneisen parameter is found from evaluating Eq. (38) using various thermodynamic identities (Zel'dovich and Raiser, 1967): $\Gamma = \beta\kappa/\rho C_p$, where β is the coefficient of volumetric expansion, κ is the adiabatic bulk modulus, ρ is the density, and C_p the specific heat at constant pressure. Normally, the dynamic Gruneisen parameter is determined from $\Gamma\rho = \Gamma_o \rho_o$ where the subscript refers to the room-temperature, zero-pressure values (McQueen, et al., 1970).

Equation (39) has certainly been shown to be valid for solids, and in particular, metals, as well as liquids. But at very high pressures, and at distended states (e.g., vaporization), Eq. (39) must be replaced by other formulas. Porous materials need special treatment (Herrmann, 1969; Carroll and Holt, 1972; 1972b). The Tillotson equation of state (Tillotson, 1962) has been used with success for impacts at hypervelocities (Sedgwick, et al., 1978). Trucano and Asay (1986) show that the form of the equation of state is very important in predicting the dynamics of the debris bubble after hypervelocity impact of a bumper shield. A conclusion of Holian and Burkett (1986) is that the ability to predict the dynamics of the debris bubble not only is dependent upon the equation of state, but the ability of the code to treat correctly two-phase flow. The reader is referred to the excellent review article by Asay and Kerley (1986) for further information on equations of state.

Constitutive Modeling

Elastic-Plastic Formulation: Figure 13a displays the pressure-volume relation (Hugoniot) if the material has no strength (hydrodynamic). However, if the material has strength, then it will load elastically until yield, at which point it will begin to permanently deform plastically. An elastic, perfectly plastic material response is shown in Fig. 13b, both for compression and tension. The "superposition" of the curves of Figs. 13a and 13b is shown in Fig. 13c for the condition of uniaxial strain. The material is seen to load elastically to the Hugoniot elastic limit, and then flow plastically parallel to the Hugoniot. Wilkins (1964, 1969) developed the methodology for the inclusion of strength effects which is used in today's finite difference and finite element hydrocodes. For the condition of uniaxial strain, the principal stresses, t_i, are given by:

$$t_1 = -P + \frac{4}{3}\tau_m \qquad t_2 = t_3 = -P - \frac{2}{3}\tau_m \qquad P = \frac{1}{3}(t_1 + t_2 + t_3) \tag{40}$$

where τ_m is the maximum shear stress, which, at plastic flow, is equal to the flow (yield) stress $Y^o/2$. The hydrostatic pressure is simply the average of the principal stresses. Thus, an applied load is carried by the hydrostatic pressure and in part by its resistance to shear (Davison and Graham, 1979). From Eqs. (40), it can be seen that if the hydrostatic pressure is very large, it is reasonable to ignore material strength, i.e., the hydrodynamic approximation.

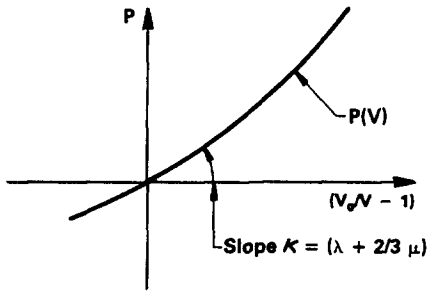

a. Hydrodynamic response.

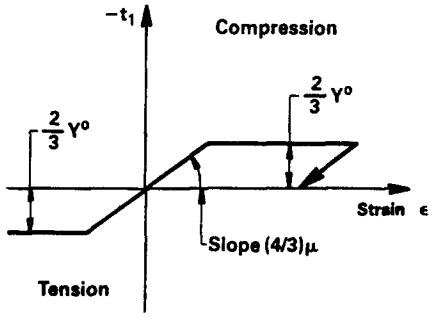

b. Elastic-perfectly plastic response.

In general, the stress can be divided into its volumetric and deviatoric parts:

$$\sigma_{ij} = -P\,\delta_{ij} + s_{ij} \tag{41}$$

The first term accounts for volumetric changes, and is obtained from the equation of state. The stress deviators, s_{ij}, are related to distortion changes, and in particular, the time rate of change of the deviators is computed from the strain rates:

$$\dot{s}_{ij} = 2G\dot{\epsilon}_{ij} + \dot{\Delta}_{ij} \tag{42}$$

where G is the shear modulus, and $\dot{\Delta}_{ij}$ is a correction for rigid body rotation.

To compute elastic-plastic flow, it is assumed that the total strains can be separated into elastic ϵ^e, and plastic ϵ^p components, giving for the strain rate tensor:

$$\dot{\epsilon}_{ij} = \dot{\epsilon}^e_{ij} + \dot{\epsilon}^p_{ij} \qquad \dot{\epsilon}^p_{ii} = 0 \qquad \dot{\epsilon}^p_{ij} = \beta s_{ij} \tag{43}$$

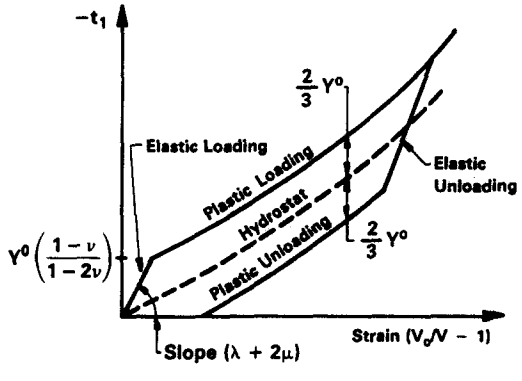

c. Combination of a. and b.

Fig. 13. Stress-strain relations in one dimension for a material with strength.

The second equation, Eq. (43b), is a statement of incompressibility of the plastic part of the strain rate. The third equation (45c) states the assumption that the plastic strain rate is proportional to the stress deviator (Wilkins, 1964):

An equivalent stress σ_{eq} can be defined from the second invariant of the deviatoric stress tensor:

$$\sigma_{eq} = (3\, s_{ij}s_{ij}/2)^{\frac{1}{2}} \qquad \sigma_{eq} \le Y^{o} \tag{44}$$

Equation (44b), the von Mises yield criterion, states that the equivalent stress must be less than or equal to the yield stress. In other words, for complex stress states, the von Mises yield criterion provides the determination if a material has flow plastically.

For computational purposes, it is first assumed that $\beta = 0$ in Eq. (43c). The stress deviators are computed from integrating Eqs. (42), and then σ_{eq} is compared to Y^{o}. If σ_{eq} is less than Y^{o}, the material is elastic; if greater than Y^{o}, the material has flowed plastically and the stresses must be allowed to relax back to the yield surface. This is done by redefining $\beta = Y^{o}/\sqrt{3s_{ij}s_{ij}/2}$. By adjusting the stress deviators in this manner, perpendicular to the yield surface, only the plastic component of the stresses are affected (Wilkins, 1964). Once the stress deviators are adjusted, the material state point will lie on the yield surface.

General Constitutive Equations in Hydrocodes: The original formulation of strength effects considered that materials were elastic, perfectly plastic. But the elastic-plastic constitutive formulation summarized in the last section is sufficiently general to permit work hardening and other effects which are very important for many materials.

Most hydrocodes have various material options. The first several options are variations of an elastic, perfectly plastic constitutive equation:

- If the yield stress Y^{o} is set to zero, the material is treated hydrodynamically.
- If Y^{o} is taken as a non-zero positive constant, then the material is treated as elastic, perfectly plastic, undergoing plastic deformation whenever $\sigma_{eq} \ge Y^{o}$.
- If Y^{o} is taken as infinity (or a very large number), the material is treated as perfectly elastic since it can never yield.

Note that three different material responses are obtained by modifying "Y^{o}". In general, this is how most material strength effects can be modeled. For example, the effects of thermal softening sometimes are approximated by

$$Y = Y^{o}\,(1 + Y_1\,\eta)\,(1 - \frac{E}{Y_2}) \tag{45}$$

where Y_1 gives an increase in the yield strength with compression and a decrease with expansion ($\eta = \rho/\rho_o - 1$), and the Y_2 term accounts for the decrease in the flow stress with increasing internal energy, with Y_2 generally taken to be the melt or sublimation energy.

Strain hardening, strain rate dependence, and temperature effects can all be incorporated into the codes by modifying the flow stress. In visco-plastic material response, the state of the material may exceed its equilibrium value due to strain-rate effects, and the stress will relax back to the yield surface (see the discussion on viscous effects in the section on shock viscosity). Strain-rate dependent stress relaxation is treated similarly to other effects by modifying the flow stress, except that the stress relaxation process requires subcycling (Herrmann, Lawrence and Mason, 1970).

Discussions of these various types of constitutive relations are given by Swegle (1978), Kipp and Lawrence (1982), and Johnson and Cook (1983). Anisotropic effects also have been considered, such as the Bauschinger effect (Kipp and Lawrence, 1982) and orthotropic materials (Johnson, Vavrick and Colby, 1980). However, there are certain limitations on constitutive models for the hydrocodes. Johnson and Cook (1983) state:

> It is recognized that more complicated models may indeed give more accurate descriptions of material behavior. Similarly, various models may give better descriptions for various materials. In many instances, however, the computational user cannot readily incorporate complicated and diverse models. The result is that a constant "dynamic flow stress" is often used.

Certainly the model must use parameters computed by the hydrocode. Davison (1984) discusses that a continuum description of phenomena must be consistent with macroscopic thermodynamic principles, and reflect the microscope basis of the phenomena to be represented. He discusses the role of internal state variables in constitutive modeling. Constitutive modeling is discussed further in the review paper by Asay and Kerley (1986), and Steinberg (1986).

Failure Modeling

Material failure modeling, within the context of the hydrodynamic codes, has evolved over the years. In recent years, it has reached levels of sophistication and complexity to predict accurately certain specific failure modes. It was recognized very early in code development that while materials can and do support high pressures in compression, it is physically untenable for materials to support large (negative) pressures or stresses in tension. The very first criterion applied in the hydrocodes was a tensile pressure or stress cutoff which "clamped" the material pressure or stress at some physically reasonable, but maximum negative value, generally referred to in the codes as σ_{min} or P_{min}. The material retained no knowledge of former "fracturing"; that is, the material was still treated as a continuum and all elements or grid points representing the material still could support tensile and shear stresses. The next level of sophistication was to set the stress to zero in a computational zone that reached a prescribed tensile fracture stress. Memory of the fracture was retained and the computational zone could no longer support tensile or shear stresses. This procedure has been applied successfully to predict and model spall (Mescall and Papirno, 1974; Shockey, Curran and De Carli, 1975; Bertholf, et al., 1975). In some Eulerian codes such as CSQII (Thompson, 1979), interior failure in tension introduces a void which results in the contraction of the surrounding matter which relieves tensions. The void can grow in size in subsequent cycles until the zone no longer exceeds the failure criterion. For computational purposes, these voids are treated as an additional "material." Voids can grow to neighboring zones and subsequently look like cracks which can coalesce and form spall (Thompson, 1979).

A variety of instantaneous "critical value" variables has been used to model instantaneous material failure, including a fracture stress, maximum principal stress, volumetric strain, maximum principal strain, shear strain, equivalent effective strain (second invariant of the strain deviator), and total plastic work. The success of each of these failure criteria, and why one might be more suitable than another, generally depends upon the material being modeled and the type of failure to be expected.

But damage typically grows with time and applied stress, and except when the intensity of the applied load is so severe that damage occurs in negligibly short time, it is unreasonable to expect satisfactory results from an instantaneous failure criteria. Zukas (1980) summarizes experimental observations that lead to the following conclusions about general features of material failure:

- o A range of damage is possible;
- o Damage grows as a function of time and the applied stress;
- o As the level of damage increases, the material is weakened and its stiffness reduced.

More complicated failure criteria have been used to account for progressive development of failures. For example, one of the earliest time-dependent models was due to Tuler and Butcher (1968) to account for the observed dependence of spall failure on stress pulse duration. Failure is assumed to occur instantaneously when a critical value of the damage, K, defined by the time integral is reached:

$$K = \int_0^t (\sigma - \sigma_o)^\lambda \, dt \tag{46}$$

where $\sigma(t)$ is the tensile stress pulse of arbitrary shape, and σ_o is a threshold stress level below which no significant damage will occur regardless of stress duration. The material constant, λ, is used to fit experimental data.

A more sophisticated fracture model was used by Bertholf, et al., (1977, 1979) to model long rod penetration into spaced armor. Briefly, the model is a biaxial fracture-stress model where the threshold plastic work, W_p, and threshold tensile stresses must be exceeded before a crack will form normal to the maximum tensile stress. The angle of fracture is retained and the normal stress decays to zero over a few computational time cycles. The orthogonal direction can also fracture.

Note that Eq. (46), when differentiated, implies that the rate of damage accumulation is a function of stress:

$$\dot{K} = (\sigma - \sigma_o)^\lambda \tag{47}$$

Criteria in which the damage accumulation is also a function of the current extent of damage, strain, and temperature have been devised by Davison, and co-workers (1973, 1977)

$$\dot{K} = f(K, \epsilon, T) \tag{48}$$

to describe more accurately the response of an elastic-viscoplastic deformation with spall damage accumulation. The work of Davison and Stevens (1973) presents a theory of spallation for the case where damage takes the form of small, penny-shaped cracks, such as those which occur in relatively brittle materials. Later work (Davison, et al., 1977, 1978, and Kipp and Davison, 1981) considered the case in which the material is very ductile and spall damage takes the form of a diffuse distribution of small spherical voids. These material descriptions have not been used extensively, but are suitable for incorporation into the numerical hydrocodes. Johnson (1982, 1985) has performed recent work with EPIC where an accumulative damage model for fracture takes into account strain, strain rate, temperature, and a dimensionless pressure which is the pressure divided by the yield stress (the yield stress is a function of strain, strain rate, and temperature).

Micromechanical behavior has been incorporated in a continuum damage model by researchers at SRI International which attempts to account explicitly for the nucleation and growth (NAG) of voids, cracks, and shear bands in ductile, brittle, and shear failure, respectively (Seaman, Curran and Shockey, 1976; Hageman and Herrmann, 1978; Erlich, Seaman, Shockey and Curran, 1980). Ductile failure damage is initiated when the average stress exceeds a tensile-pressure criterion. Brittle failure is initiated when the maximum normal stress exceeds a tensile threshold. Shear banding begins when the plastic shear strain exceeds a critical value. After initiation, voids, cracks, or shear bands nucleate and grow according to experimentally determined rate equations. As damage accumulates, the stresses are relaxed by amounts and in direction governed by the damage distribution functions (the damage distribution functions, e.g., crack, void or shear band size and orientation are treated as internal state variables). The ductile and brittle fragmentation (FRAG) and shear banding (SNAG) have been used to predict fragment size distributions. However, as shown by the work of Mock and Holt (1982, 1983), considerable time and effort are required to determine the dynamic fracture parameters required by the models. Indeed, except for very few materials, the NAG/FRAG/SNAG models are not used because the dynamic fracture parameters are not known, and to obtain them requires a major research effort.

Lagrangian Hydrocode Modeling of Deep Penetration: Over the last several years, considerable effort has been focused on improving the ability of Lagrangian hydrocodes to compute the entire history of a penetrating projectile. Generally, the realm of penetration and perforation has been studied with Eulerian codes because of the severe grid distortion of Lagrangian calculations. But the advantages inherent in a Lagrangian code, as discussed earlier, has provided the impetus for finding ways to perform penetration calculations with a Lagrangian code. The first attempt to extend the time solution of an impact event with Lagrangian hydrocodes utilized rezoning procedures. This approach has been successfully applied to impact problems (Bertholf, et al., 1977, 1979), but can be manhour and computer intensive.

The first approach to allow deep penetration into thick targets using a Lagrangian code by modifying the slideline algorithms was performed by G. Johnson using EPIC-3 (Johnson, et al.; 1980; Johnson, 1982). The target material was allowed to fail completely and the master surface redefined to include the next layer of grid points. The failure had to be along a predetermined region. A number of approximations and assumptions had been made which were not particularly satisfying; thus, it was not used extensively.

In a very real sense, the ability to model deep penetration is dependent on physically realistic failure modeling. In EPIC (2 or 3), material fracture has been handled by failing elements in one of two ways. Partial failure occurs when an element is predicted to fracture by a cumulative damage model (Johnson and Cook, 1985). When this type of failure occurs, no tensile or shear stresses are allowed to develop in the failed element, but the element can support hydrostatic compression. A second option for treating failure is to set all stresses (including the pressure) to zero. This is called total failure (or erosion). The element essentially dissappears except mass is retained at the nodes (Johnson and Stryk, 1986). Normally, sliding surfaces are used at the projectile/target interface. Techniques have been developed to handle dynamic relocation of sliding surfaces to model two types of failure which can occur with penetration--adiabatic shear, and erosion--depending upon the velocity of the projectile and material strengths. Each will be discussed below.

Adiabatic Shear: During a penetration event, as target material is being "pushed" by the projectile, the work of plastic deformation is converted almost entirely into heat. Because of the high deformation rates, this heat is unable to conduct away from the plastic zone, resulting in an increase in temperature in the plastic zone. This leads to additional local plastic flow, concentrating the local plastic strain even further (Trucano and Grady, 1984). It is usually envisioned that plastic shear instabilities are initiated at sites of stress concentration in an otherwise uniformly straining solid (Burns, et al., 1981). The result is the propagation of a narrow band of intense plastic strain through the material along planes of maximum shear stress or minimum strength until unloading occurs or the material fractures. Called adiabatic shear, this mechanism is present in most impact scenarios, though other physical processes can

dominate. For striking velocities near the ballistic limit (perforation) velocity of a "thick" target, an intact plug will result (Wilkins, 1978; Zukas, 1980).

Ringers (1983) at BRL has modified EPIC-2 (Johnson, 1978b) to allow for deep penetration when the failure mode is target plugging. Essentially, a new node is generated by splitting a node, and the master slide surface is effectively redefined. This redefinition of the slide surface is referred to as dynamic relocation. Certain criteria establish whether a node can split. Considerable work was required to establish the criteria for the splitting of a node (which must be on the master surface), and the direction of the split. A number of approaches were found to be intractable; at the same time, a definite attempt was made to keep the criteria physical and reasonable. The criterion adopted was that a split would occur when the equivalent strain reached a specified critical level and the shear stress was greater than the axial or radial deviator stresses. The direction of the split was determined by the strain of the element that had met the criteria for splitting. If the magnitude of the axial strain was greater than the magnitude of the radial strain, splitting was to the nearer radial node; otherwise, splitting was to the nearer axial node.

To account for "sliding" between the two sides of the split which develops in the target, another set of master and slave surfaces was established between the developing plug and remaining target material. This second master/slave surface allows for the plug material elements to "slide" past the remaining target material--this is readily visible in Fig. 14.

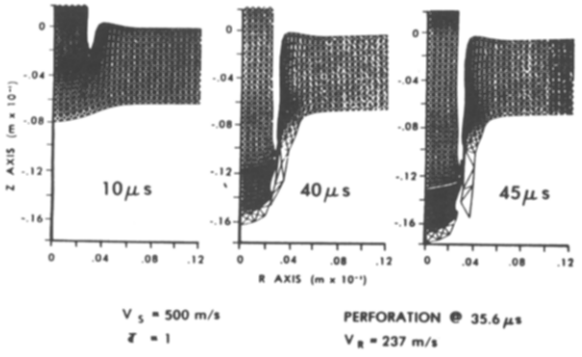

Fig. 14. Deep Penetration by a Lagrangian calculation--adiabatic shear (from Ringers, 1983).

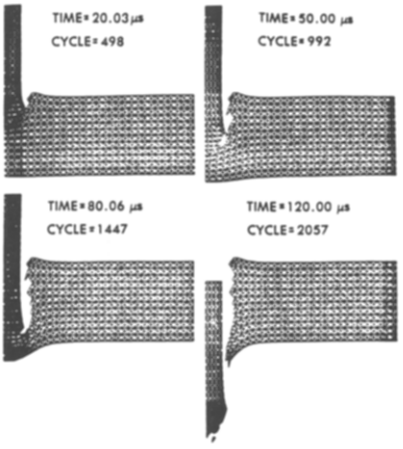

Fig. 15. Plate perforation by a lagrangian calculation--erosion (courtesy of Kimsey and Zukas).

Erosion: The failure mode is significantly different for hypervelocity impact where the impact pressures substantially exceed material strength. In hypervelocity impact, the principal factor in characterizing material behavior is the high pressure equation of state. Material response is characterized by large strains and total failure generally referred to as erosion (both for the target and the penetrator). The resulting material flows are similar to colliding water jets, hence the term "hydrodynamic."

The fundamental difference, from the computational viewpoint of modeling failure by erosion as opposed to adiabatic shear, is the treatment of the slidelines. In the plugging mode, the slideline is redefined to follow the failure surface, e.g., the separating of elements by the splitting of nodes. However, with erosion, the sliding surfaces are redefined in the presence of total element failure. These two approaches tend to mimic the physical processes one might heuristically expect for the two failure modes.

Kimsey and Zukas (1986) developed an algorithm for EPIC-2 to allow redefinition of the master surface and a symmetric treatment of the master-slave interface. The procedure is based on discrete master segments, removing the criteria for a continuous master surface. Failure of both the target and penetrator is modeled. Figure 15 shows the results obtained for penetration of a steel plate by a 65 gram, hemispherically nosed steel rod with a striking velocity of 1103 m/s. A plot of the number of cycles versus time (microseconds) is approximately linear, implying that the computational time step is essentially a constant. Kimsey and Zukas also conducted the numerical simulation of a long rod penetrator impacting a semi-infinite target at 3.1 km/s. They obtained excellent agreement with experiment (Kimsey and Zukas, 1986).

Belytschko and Lin (1985, 1986) used a different approach for erosion using EPIC-3. Their algorithm requires no definition or tracking of sliding interfaces. The interaction is handled by operations on slave nodes and master elements. Hexahedral elements were introduced to simplify the interaction algorithm, and hourglass or keystone viscosity was required to stop spurious deformation modes caused by one point-integration.

Strecher and Johnson (1984) modified EPIC-2 to have an eroding interface. The normal impact of a 5 km/s tungsten projectile into a semi-infinite steel target is shown in Figure 16. Johnson and Styrk (1986) also have modified EPIC-3 to account for total material failure in the projectile and target. Their algorithm redefines the sliding interface.

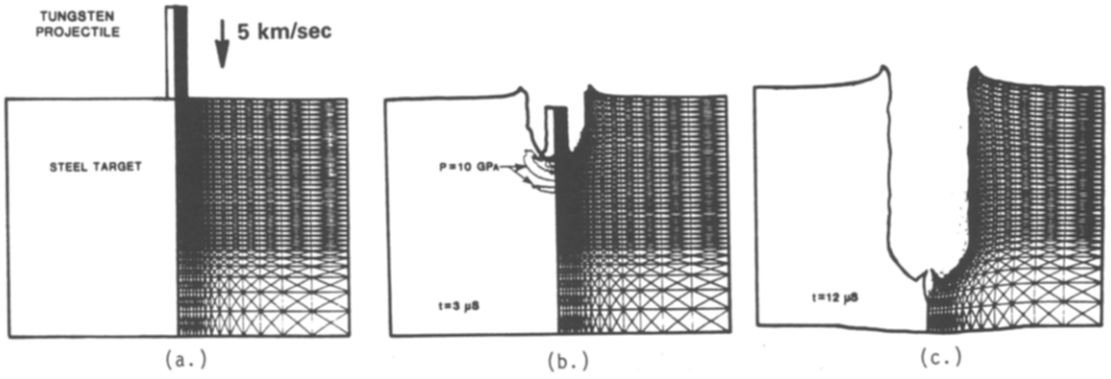

Fig. 16. Deep penetration into a semi-infinite target--erosion (courtesy of G. Johnson).

Summary of Deep Penetration Modeling: In conclusion, note two important considerations with respect to these two failures, shear failure and erosion. First, the dominant mode of failure has been assumed. Work to date has been to understand and realistically model a specific failure mechanism; the transition from one failure mode to another is generally beyond current predictive capabilities. Second, adiabatic shear failure is more complex to model, requiring failure criteria (some reasonable criteria did not work), a procedure for extrapolating the direction of failure, and separation of material along the failure plane. Erosion is characterized by a much simpler failure mechanism, consistent with the previous subsection discussion that when damage levels are high, failure is easier to characterize. However, though one type of failure may be more complex to model, implementation of the failure model into the computer program can be as difficult or even more difficult for the simpler model, particularly where element or node removal may be desired, or relocation of slidelines is required. Certainly implementation of either of these failure models required a substantial effort and detailed knowledge of the computer program logic.

Summary of Material Failure Modeling

In summary, the most used models to predict material failure in hydrocode simulations require some critical stress, strain, plastic work or other instantaneous criteria, mostly because some appropriate critical level can be estimated from known material properties. As long as the conditions for failure are far above the threshold, damage occurs in negligible times and these single-criterion models are generally adequate. However, near threshold, a time-dependent description of failure growth is required (with a threshold below which no damage occurs); these models realistically predict increasing damage rates as the threshold is exceeded. If the threshold is exceeded by a sufficiently large quantity, the damage rate saturates and the model effectively can be replaced by a single criterion, sudden damage model. Realistic numerical modeling of failure near thresholds also requires a fine grid mesh, and attendant smaller time step, to resolve accurately the physical state of the material such as the stresses (e.g., reference Bertholf, et al. (1975) who found that a high degree of numerical resolution was required to predict the back-surface spallation observed in an impact experiment--coarse zoning resulted in a solution which predicted no back-surface spallation). Thus, the numerical analyst must exercise judgement to obtain an acceptable answer. The detail necessary, and the complexity of the failure model, is failure-mode dependent. Also, the numerical analyst must foresee the dominate failure mode expected since state of the art in failure modeling *a priori* assumes a failure mode and then tries to predict that failure mode from basic principles. These last two points are vividly demonstrated in the last section where two different failure mechanisms encountered in penetration and perforation are modeled explicitly in a hydrocode.

SUMMARY

Hydrocodes are large computer programs used to simulate numerically highly dynamic events, particularly those involving shocks, by solving the conservation equations coupled with material descriptions. The equations are discretized, using either the finite difference or finite element technique. The conservation equations can be written in one of two mathematical descriptions, Eulerian (spatial) or Lagrangian (material), and each of these descriptions has advantages and disadvantages. In particular, Lagrangian codes provide good spatial resolution relative to the number of grid cells needed to describe the problem; free surfaces and material interfaces are well defined. Finally, because they are written in material coordinates, Lagrangian codes can provide excellent material constitutive modeling. However, severe distortion of the grid sometimes limits the usefulness of the Lagrangian codes to early times. Eulerian codes, because of their fixed coordinate systems, can handle problems where large distortions take place, at the expense of the attractive features of Lagrangian codes (grid economy, interfaces, material descriptions).

The formulation of the numerical algorithms to solve the conservation equations require specific treatments to ensure numerical stability (a limiting integration time step), and unwanted large oscillations at shock discontinuities (artificial viscosity). A trade-off in efficiency versus accuracy has led to the codes as they are today, and also has led to the development of specific algorithms to take advantage of Eulerian-like and Lagrangian-like attributes (Johnson and Anderson, 1986).

The hydrocode codes have been very useful in understanding and predicting transient phenomena which occur on the order of microseconds and tens of microseconds. Two-dimensional codes have been in existence since the early-to-mid 60's and their sophistication has continued to grow during the 70's and early 80's. The advent of the larger (more memory) and faster computers have allowed three-dimensional versions of the codes to be formulated and solutions obtained (Johnson and Anderson, 1986). Since the development of a specific code usually has grown out of a particular need, some of the codes have enhanced features in certain areas; for example, the coupling of radiation effects in the codes developed by Sandia Laboratories. Zukas (1980) has described the major physical weakness of the codes to be their material descriptions. It is true that the numerical simulation can only be as accurate as the material models. Traditional material parameters consisted of static or slow strain-rate parameters measured in the laboratory. However, an active research area has been the measurement and understanding of high strain-rate phenomena, and our understanding of material response has improved considerably. But obviously, there are still challenges.

In recent years, considerable efforts have been spent on post-processing, particularly in the graphical display of data. The output from the hydrocodes can be voluminous, and the only hope for assimilation is by an appropriate graphical display of the data. Indeed, these graphic routines can become "monster" programs themselves. An undesirable outgrowth of improved pre- and post-processing packages is that many people who do not (or do not want to) understand the "physics" can now use the codes. This is leading to an emphasis on impressive graphics, movies, etc., opposed to analysis and understanding of the numerical results.

Hydrocodes can be very powerful tools in research if one recognizes their limitations and understands their operations. They can give detailed understanding of physical processes and can be used to perform analytical experiments. These computational experiments can be cheaper than laboratory experiments, and, in some cases, because the actual experiment is extremely difficult or impossible to perform, offer the only viable way to obtain information.

REFERENCES

_____(1980). "Materials Response to Ultra-High Loading Rates," U.S. National Materials Advisory Board, Washington, DC.

Asay, J. R., and G. I. Kerley (1986). "The Response of Materials to Dynamic Loading," International Journal of Impact Engineering, Vol. 5.

Becker, R. (1922). "Stosswelle and Detonation," Z. Physik, Vol. 8, p. 321.

Belytschko, T. (1974). "Finite Element Approach to Hydrodynamics and Mesh Stabilization," in Computational Methods in Nonlinear Mechanics, edited by J. T. Oden et al., Texas Institute for Computational Mechanics, pp. 231-238.

Belytschko, T. (1975). "Nonlinear Analysis--Descriptions and Numerical Stability," in Computer Programs in Shock and Vibration, edited by W. and B. Pilkey, Shock and Vibration Information Center, Washington, DC., pp. 537-562.

Belytschko, T. (1976). "Computer Methods in Shock and Wave Propagation Analysis," in Computing in Applied Mechanics, AMD-Vol. 18, American Society of Mechanical Engineers, pp. 139-161.

Belytschko, T., R. L. Chiapetta, and H. D. Bartel (1976). "Efficient Large Scale Nonlinear Transient Analysis by Finite Elements," International Journal for Numerical Methods in Engineering, Vol. 10, pp. 579-596.

Belytschko, T., and J. I. Lin (1985). " A New Interaction Algorithm with Erosion for EPIC-3," BRL-CR-540, USA Ballistic Research Laboratory, Aberdeen Proving Ground, MD.

Belytschko, T., and J. I. Lin (1986). "A Three Dimensional Impact-Penetration Algorithm with Erosion," International Journal of Impact Engineering, Vol. 5.

Belytschko, T., W. K. Liu, J. M. Kennedy and S. J. Ong (1984). "Hourglass Control in Linear and Nonlinear Problems," Computer Methods in Applied Mechanics and Engineering, Vol. 43, pp. 251-276.

Bertholf, L. D., L. D. Buxton, B. J. Thorne, R. K. Byers, A. L. Stevens, and S. L. Thompson (1975). "Damage in Steel Plates from Hypervelocity Impact II. Numerical Results and Spall Measurement," Journal of Applied Physics, Vol. 46, No. 9, pp. 3776-3783.

Bertholf, L. D., M. E. Kipp, and W. T. Brown (1977). "Two-Dimensional Calculations for the Oblique Impact of Kinetic Energy Projectiles with a Multi-Layered Target," BRL-CR-333, USA Ballistic Research Laboratory, Aberdeen Proving Ground, Maryland.

Bertholf, L. D., M. E. Kipp, W. T. Brown, and A. L. Stevens (1979). "Kinetic Energy Projectile Impact on Multi-Layered Targets: Two-Dimensional Stress Wave Calculations," ARBRL-CR-00391, USA Ballistic Research Laboratory, Aberdeen Proving Ground, Maryland.

Burns, T. J., D. E. Grady, and L. S. Costin (1981). "On a Criterion for Thermo-Plastic Shear Instability," in Shock Waves in Condensed Matter--1981, edited by W. J. Nesslis, L. Seaman and R. A. Graham, American Institute of Physics, pp. 372-375.

Carroll, M. M. and A. C. Holt (1972). "Suggested Modifications of the P-alpha Model for Porous Materials," Journal of Applied Physics, Vol. 43, No. 2, pp. 759-761.

Carroll, M. M., and A. C. Holt (1972). "Static and Dynamic Pore Collapse Relations for Ductile Porous Materials," Journal of Applied Physics, Vol. 43, No. 4, pp. 1626-1636.

Chiapetta, R., T. Belytschko, and J. Rouse (1973). "A Computer Code for Dynamic Stress Analysis of Media-Structure Problem with Nonlinearities (SAMSON)," Report AFWL-TR-72-104, Air Force Weapons Laboratory, Kirtland AFB, NM.

Courant, R., K. O. Friedrichs, and H. Lewy (1928). "Uber die partiellen Differenzengleichungen der mathematischen Physik," Mathematische Annalen, Vol. 100, pp. 32-74.

Davison, L. (1984). "Numerical Modeling of Dynamic Material Response," in Shock Waves in Condensed Matter--1983, edited by J. R. Asay, R. A. Graham, and G. K. Straub, Elsevier Science Publishers, pp. 181-186.

Davison, L. W., and R. A. Graham (1979). "Shock Compression of Solids," Physics Reports, Vol. 55, No. 4, pp. 257-379.

Davison, L., and M. E. Kipp (1978). "Calculation of Spall Damage in Ductile Metals," in High Velocity Deformation of Solids, K. Kawata and J. Shioiri, eds., Springer-Verlag, West Berlin, Germany.

Davison, L. W., and A. L. Stevens (1973). "Thermomechanical Constitution of Spalling Elastic Bodies," Journal of Applied Physics, Vol. 44, No. 2, pp. 668-674.

Davison, L. W., A. L. Stevens, and M. E. Kipp (1977). "Theory of Spall Damage Accumulation in Ductile Metals," J. Mech. Phys. Solids, Vol. 25, pp. 11-28.

Drumheller, D. S. (1986). "Hypervelocity Impact of Mixtures," International Journal of Impact Engineering, Vol. 5.

Emery, A. F. (1967). "An Evaluation of Several Differencing Methods for Inviscid Fluid-Flow Problems," SCL-DC-66-78, Sandia National Laboratories, Albuquerque, NM.

Erlich, D. C., L. Seaman, D. A. Shockey, and D. R. Curran (1980). "Development and Application of a Computational Shear Band Model," ARBRL-CR-00416, USA Ballistic Research Laboratory, Aberdeen Proving Ground, Maryland.

Goudreau, G. L. and J. O. Halquist (1982). "Recent Developments in Large-Scale Finite Element Lagrangian Hydrocode Technology," Computer Methods in Applied Mechanics and Engineering, Vol. 33, pp. 725-757.

Hageman, L. J., and R. G. Herrmann (1978). "Incorporation of the NAG-FRAG Model for Ductile and Brittle Fracture into HELP, a 2D Multimaterial Eulerian Program," ARBRL-CR-00380, USA Ballistic Research Laboratory, Aberdeen Proving Ground, Maryland.

Halquist, J. O. (1976). "A Procedure for the Solution of Finite-Deformation Contact-Impact Problems by the Finite Element Method," Report UCRL-52066, Lawrence Livermore National Laboratory, Livermore, CA.

Halquist, J. O. (1976b). "Preliminary User's Manual for DYNA3D and DYNAP--Nonlinear Dynamic Analysis of Solids in Three Dimensions," UCID-17268, Lawrence Livermore National Laboratory, Livermore, CA.

Halquist, J. O. (1978). "DYNA2D--An Explicit Finite Element and Finite Difference Code for Axisymmetric and Plane Strain Calculations (User's Guide)," UCRL-52429, Lawrence Livermore National Laboratory, Livermore, CA.

Herrmann, W., (1969). "Constitutive Equation for the Dynamic Compaction of Ductile Porous Materials," Journal of Applied Physics, Vol. 40, No. 6, pp. 2490-2499.

Herrmann, W. (1975). "Nonlinear Transient Response of Solids," in Shock and Vibration Computer Programs, Reviews and Summaries, edited by W. and B. Pilkey, Shock and Vibration Information Center, Washington, D.C, pp. 151-172.

Herrmann, W. (1977). "Current Problems in the Finite Difference Solution of Stress Waves," in Proceedings of the Workshop on Nonlinear Waves in Solids, edited by T.C.T. Ting, R. J. Clifton and T. Belytschko, sponsored by US Army Research Office and National Science Foundation, pp. 31-52.

Herrmann, W., R. J. Lawrence, and D. S. Mason (1970). "Strain Hardening and Strain Rate in One-Dimensional Wave Propagation Calculations," SC-RR-70-471, Sandia National Laboratories, Albuquerque, NM.

Hildebrand, F. B., (1962). Advanced Calculus for Applications, Prentice-Hall, Inc.

Holian, K. S., and M. W. Burkett (1986). "Sensitivity of Hypervelocity Impact Simulations to Equation of State," International Journal of Impact Engineering, Vol. 5.

Johnson, G. R. (1976). "Analysis of Elastic-Plastic Impact Involving Severe Distortions," Journal of Applied Mechanics, Vol. 43, No. 3, pp. 439-444.

Johnson, G. R. (1977). "A New Computational Technique for Intense Impulsive Loads," Proceedings of the Third International Symposium on Ballistics, Karlsruhe, Germany.

Johnson, G. R. (1977b). "High Velocity Impact Calculations in Three Dimensions," Journal of Applied Mechanics, Vol. 99, No. 1, pp. 95-100.

Johnson, G. R. (1977c). "EPIC-3, A Computer Program for Elastic-Plastic Impact Calculations in 3 Dimensions," Contract Report No. 343, USA Ballistic Research Laboratory, Aberdeen Proving Ground, MD.

Johnson, G. R. (1978b). "EPIC-2, A Computer Program for Elastic-Plastic Impact Calculations in 2 Dimensions Plus Spin," ARBRL-CR-00373, US Army Ballistic Research Laboratory, Aberdeen Proving Ground, MD.

Johnson, G. R. (1982). "Status of the EPIC Codes, Material Characterization and New Computing Concepts at Honeywell," in Computational Aspects of Penetration Mechanics, Springer-Verlag.

Johnson, G. R., D. D. Colby, and D. J. Vavrick (1979). "Three Dimensional Computer Code for Dynamic Response of Solids to Intense Impulsive Loads," International Journal for Numerical Methods in Engineering, Vol. 14, pp. 1865-1871.

Johnson, G. R., and W. H. Cook (1983), "A Constitutive Model and Data for Metals Subjected to Large Strains, High Strain Rates and High Temperatures," Proceedings of the Seventh International Symposium on Ballistics.

Johnson, G. R., and W. H. Cook (1985). "Fracture Characteristics of Three Metals Subjected to Various Strains, Strain Rates, Temperatures and Pressures," Engineering Fracture Mechanics, Vol. 21, No. 1, pp. 31-48.

Johnson, G. R., and R. A. Stryk (1986). "Eroding Interface and Improved Tetrahedral Element Algorithms for High Velocity Impact Computations in Three Dimensions," International Journal of Impact Engineering, Vol. 5.

Johnson, G. R., D. J. Vavrick, and D. D. Colby (1980). "Further Development of EPIC-3 for Anisotropy, Sliding Surfaces, Plotting and Material Models," Contract Report ARBRL-CR-00429, USA Ballistic Research Laboratory, Aberdeen Proving Ground, Maryland.

Johnson, W. E. (1986). Personal communication.

Johnson, W. E. and C. E. Anderson (1986). "History and Application of Hydrocodes to Hypervelocity Impact," International Journal of Impact Engineering, Vol. 5.

Jonas, G. H., and J. A. Zukas (1978). "Mechanics of Penetration: Analysis and Experiment," International Journal of Engineering Science, Vol. 16, No. 11, pp. 879-904.

Karpp, R. R. (1972). "The Method of Characteristics," in Dynamic Response of Material to Intense Impulsive Loading, P. C. Chou and A. K. Hopkins, eds., Air Force Materials Laboratory, Ohio.

Kerley, G. I. (1986). "Theoretical Equation of State for Aluminum," International Journal of Impact Engineering, Vol. 5.

Key, S. W. (1974). "HONDO - A Finite Element Computer Program for the Large Deformation Dynamic Response of Axisymmetric Solids," SLA-74-0039, Sandia National Laboratories, Albuquerque, NM.

Key, S. W. (1974b). "A Finite Element Procedure for Large Deformation Dynamic Response of Axisymmetric Solids," Computer Methods of Applied Mechanics and Engineering, Vol. 4, pp. 195-218.

Key, S. W., Z. E. Beisinger and R. D. Krieg (1978). "HONDO II - A Finite Element Computer Program for Large Deformation Dynamic Response of Axisymmetric Solids," SLA-78-0422, Sandia National Laboratories, Albuquerque, NM.

Kimsey, K. D., and J. A. Zukas (1986). "Contact Surface Erosion for Hypervelocity Problems," BRL-MR-3495, USA Ballistic Research Laboratory, Aberdeen Proving Ground, MD.

Kipp, M. E., and L. Davison (1981), "Analysis of Ductile Flow and Fracture in Two Dimensions," SAND 81-0070C, Sandia National Laboratories, Albuquerque, New Mexico.

Kipp, M. E., and R. J. Lawrence (1982). "WONDY V--A One-Dimensional Finite-Difference Wave Propagation Code," SAND 81-0930, Sandia National Laboratories, Albuquerque, New Mexico

Lax, P. D. (1954). "Weak Solutions of Nonlinear Hyperbolic Equations and Their Numerical Computation," Communications on Pure and Applied Mathematics, Vol. 7, pp. 159-193.

Lax, P. D., and R. D. Richtmyer (1956). "Survey of the Stability on Linear Finite Difference Equations," Communications on Pure and Applied Mathematics, Vol. 9, pp. 267-293.

Lax, P. D., and B. Wendroff (1960). "Systems of Conservation Laws," Communications on Pure and Applied Mathematics, Vol. 13, pp. 217-237.
McQueen, R. G., S. P. Marsh, J. W. Taylor, and J. N. Fritz (1970). "The Equation of State of Solids from Shock Wave Studies," in High Velocity Impact, edited by R. Kinslow, Academic Pr.
Mescall, J. F. (1974). "Shock Wave Propagation in Solids," in Structural Mechanics Computer Programs, W. Pikley, S. Saczalski, and H. Schaeffer, editors, University of Virginia Press, VA.
Mescall, J. F. and Papirno, R. P., (1974). "Spallation in Cylinder-Plate Impact," Experimental Mechanics, Vol. 14, No. 7, p. 257-266.
Mock, W. Jr., and W. H. Holt (1982). "Determination of Dynamic Fracture Parameters for HF-1 Steel," Journal of Applied Physics, Vol. 53, No. 8, pp. 5660-5668.
Mock, W. Jr., and W. H. Holt (1983), "Fragmentation Behavior of Armo Iron and HF-1 Steel Explosive-Filled Cylinders," Journal of Applied Physics, Vol. 54, No. 5, pp. 2344-2351.
Potter, D. (1973). Computational Physics, John Wiley & Sons.
Rice, M. H., R. G. McQueen, and Walsh (1958). "Compression of Solids by Strong Shock Waves," in Solid State Physics, Vol. 6, edited by Seitz and Turnball, Academic Press.
Richtmyer, R. D., and K. W. Morton (1967). Difference Methods for Initial-Value Problems, 2nd edition, Interscience Publishers, New York.
Ringers, B. E. (1983). "New Sliding Surface Techniques Enable the Simulation of Target Plugging Failure," ARBRL-TR-02541, USA Ballistic Research Laboratory, Aberdeen Proving Ground, MD.
Roache, P. J. (1972). Computational Fluid Mechanics, Hermosa Publishers, Albuquerque, NM.
Seaman, L., D. R. Curran, and D. A. Shockey (1976). "Computational Models for Ductile and Brittle Fracture," Journal of Applied Physics, Vol. 47, No. 11, pp. 4814-4826.
Sedgwick, R. T., L. J. Hageman, R. G. Herrmann and J. L. Waddell (1978). "Numerical Investigations in Penetration Mechanics," International Journal of Engineering Science, Vol. 16, No. 11, pp. 859-870.
Shockey, D. A., D. R. Curran, and P. S. De Carli (1975). "Damage in Steel Plates from Hypervelocity Impact. I. Physical Changes and Effects of Projectile Material," Journal of Applied Physics, Vol. 46, No. 9, pp. 3766-3775.
Stecher, F. P. and G. R. Johnson (1984). "Lagrangian Computations for Projectile Penetration into Thick Plates," in Computers in Engineering 1984, edited by W. A. Graver, AMSE, NY.
Steinberg, D. J. (1986). "Constitutive Models Used in Computer Simulation of Time-Resolved, Shock-Wave Data," International Journal of Impact Engineering, Vol. 5.
Swegle, J. W. (1978). "TOODY IV--A Computer Program for Two-Dimensional Wave Propagation," SAND-78-0552, Sandia National Laboratories, Albuquerque, New Mexico.
Swegle, J. W., and D. E. Grady (1985). Shock Viscosity and the Prediction of Shock Wave Rise Times," Journal of Applied Physics, Vol. 58, No. 2, pp. 692-701.
Thompson, S. L. (1979). "CSQII--An Eulerian Finite Difference Program for Two-Dimensional Material Response - Part 1. Material Sections," SAND77-1339, Sandia National Laboratories, Albuquerque, New Mexico.
Thompson, S. L. (1986). Personal communication.
Tillotson, J. H. (1962). "Metallic Equations of State for Hypervelocity Impact," Report GA-3216, General Atomic, San Diego, CA.
Trucano, T. G., and J. R. Asay (1986). "Effects of Vaporization on Debris Cloud Dynamics," International Journal of Impact Engineering, Vol. 5.
Trucano, T. G., and D. E. Grady (1984). "Intermediate Velocity Penetration of Steel Spheres into Deep Aluminum Targets," in Shock Waves in Condensed Matter--1983, edited by J. R. Asay, R. A. Graham, and G. K. Straub, Elsevier Science Publishers, pp. 187-190.
Tuler, F. R., and B. M. Butcher (1968). "A Criterion for the Time Dependence of Dynamic Fracture," International Journal of Fracture Mechanics, Vol. 4, pp. 431-437.
von Neumann, J., and R. D. Richtmyer (1950). "A Method for the Numerical Calculation of Hydrodynamic Shocks," Journal of Applied Physics, Vol. 21, No. 3, pp. 232-237.
Walsh, R. T. (1972). "Finite-Difference Methods," in Dynamic Response of Materials to Intense Impulsive Loading, P. C. Chou and A. K. Hopkins, eds., Air Force Materials Laboratory, Ohio.
Wilkins, M. L. (1964). "Calculations of Elastic-Plastic Flow," in Methods of Computational Physics, Vol. 3, edited by B. Adler, S. Fernback, and M. Rotenberg, Academic Press, New York.
Wilkins, M. L. (1969). "Calculation of Elastic-Plastic Flow," UCRL-7322, Rev. 1, Lawrence Livermore National Laboratory, Livermore, CA.
Wilkins, M. L. (1978). "Mechanics of Penetration and Perforation," International Journal of Engineering Science, Vol. 16, No. 11, pp. 793-808.
Zel'dovich, Y. B., and Ya. P. Raiser (1967). Physics of Shock Waves and High-Temperature Hydrodynamic Phenomena, Vol. II, edited by W. D. Hayes and R. F. Probstein, Academic Press.
Zukas, J. A. (1980). "Impact Dynamics: Theory and Experiment," ARBRL-TR-02271, USA Ballistics Research Laboratory, Aberdeen Proving Ground, MD.
Zukas, J. A., G. H. Jonas, K. D. Kimsey, J. J. Misey, and T. M. Sherrick (1981). "Three-Dimensional Impact Simulations: Resources and Results," in Computer Analysis of Large-Scale Structures, edited by K. C. Parck and R. F. Jones, Jr., AMD, Vol. 49, American Society of Mechanical Engineers.
Zukas, J. A., T. Nicholas, H. F. Swift, L. B. Greszczuk, and D. R. Curran (1982). Impact Dynamics, John Wiley and Sons.